Computational study of the $CF_4/CHF_3/H_2/Cl_2/O_2/HBr$ gas phase plasma chemistry

Reference:

Tinck Stefan, Bogaerts Annemie.- Computational study of the $CF_4/CHF_3/H_2/Cl_2/O_2/HBr$ gas phase plasma chemistry

Journal of physics: D: applied physics - ISSN 0022-3727 - 49:19(2016), 195203

Full text (Publishers DOI): http://dx.doi.org/doi:10.1088/0022-3727/49/19/195203

Computational Study of the $CF_4/CHF_3/H_2/Cl_2/O_2/HBr$ Gas Phase Plasma Chemistry

Stefan Tinck and Annemie Bogaerts

Research Group PLASMANT, Dept. of Chemistry, University of Antwerp, Universiteitsplein 1, B-2610 Antwerp, Belgium

Abstract. A modelling study is performed of high-density low-pressure inductively coupled $CF_4/CHF_3/H_2/Cl_2/O_2/HBr$ plasmas under different gas mixing ratios. A reaction set describing the complete plasma chemistry is presented and discussed. The gas fraction of each component in this mixture is varied to investigate the sensitivity of the plasma properties, like electron density, plasma potential and species densities, towards the gas mixing ratios. This research is of great interest for microelectronics applications because these gases are often combined in 2-(or more-)component mixtures, and mixing gases or changing the fraction of a gas can sometimes yield unwanted reaction products or unexpected changes in the overall plasma properties due to the increased chemical complexity of the system. Increasing the CF_4 fraction produces more F atoms for chemical etching as expected, but also more prominently lowers the density of Cl atoms, resulting in an actual drop in the etch rate under certain conditions. Furthermore, CF_4 decreases the free electron density when mixed with Cl_2. However, depending on the other gas components, CF_4 gas can also sometimes enhance free electron density. This is the case when HBr is added to the mixture. The addition of H_2 to the gas mixture will lower the sputtering process, not only due to the lower overall positive ion density at higher H_2 fractions, but also because more H^+, H_2^+ and H_3^+ are present and they have very low sputter yields. In contrast, a larger Cl_2 fraction results in more chemical etching but also in less physical sputtering due to a smaller abundance of positive ions. Increasing the O_2 fraction in the plasma will always lower the etch rate due to more oxidation of the wafer surface and due to a lower plasma density. However, it is also observed that the density of F atoms can actually increase with rising O_2 gas fraction. This is relevant to note because the exact balance between fluorination and oxidation is important for fine-tuning the overall etch rate and for control of the sidewall profile.

Finally, HBr is often used as a chemical etcher, but when mixed with F- or Cl-containing gases, HBr creates the same diluting effects as Ar or He, because a higher fraction results in less chemical etching but more (physical) sputtering.

I. Introduction

Electronic components in integrated circuits have continuously been manufactured with smaller sizes during the last decades, following Moore's law.[1] High-density low-pressure plasma etching and deposition are very common techniques for creating these components with nanoscale resolution. Halogen-containing gases have been used regularly during the past decades for the plasma etching of Si, because F, Cl and Br chemically react with Si to form volatile products, in the form of SiF_4, $SiCl_4$ and $SiBr_4$, respectively. These plasmas can give rise to very high etch rates, which is cost efficient. However, due to their chemically reactive nature, in some cases, additional gases are inserted as well, to fine-tune the etching process. For example, Cl_2 gas is often accompanied by O_2, so that during the etching of trenches or vias, the sidewalls are protected with a SiO_x layer, and the bottom is etched/sputtered due to ion bombardment. Oxygen is therefore needed to control the shape of the trenches and to prevent undercutting, which is the undesired effect where Si is removed chemically underneath the mask material.

Cl_2/O_2 plasmas used for Si etching were very popular in the 90's and 00's, but due to the continuous shrinking of electronic devices, more etch control was desired and CF_4-based plasmas became at least equally popular.[2-9] The CF_4 feed gas dissociates in the plasma, yielding a large portion of chemically reactive F atoms to etch the Si, resulting in high etch rates. When including O_2, a CF_xO_y passivation layer is formed to protect the trenches from lateral etching.[10-11] A similar mechanism is found with a SF_6/O_2 gas mixture, although here, the passivation layer is only formed when the surface is at very low temperature, e.g. -100 °C.[12] The etch process can be further fine-tuned by adding a fraction of hydrogen in the form of CHF_3, CH_2F_2, CH_3F, CH_4 or simply H_2. Hydrogen is less reactive towards Si compared to the halogens, so changing the ratio between hydrogen and fluorine (and oxygen) in the gas mixture allows for a high control during plasma processing.[13]

As mentioned earlier, the most popular halogens for Si etching are F, Cl and Br, where F is more reactive than Cl and Br is the least reactive. In early chip development, F and Cl were therefore more popular, because of the higher etch rate that could be obtained compared to Br-based plasmas.

However, recently, Br-containing plasmas have seen a boost in popularity due to the ultra-small scale components found in integrated circuits. Indeed, when features are below 20 nm in size, it is more interesting to have a less aggressive etching plasma towards Si. Due to the lower reactivity of Br, the etching of very thin layers can be more properly controlled.

All the gases mentioned so far can be used in pure form, or in any combination to achieve the desired etching process. Furthermore, a noble gas like Ar or He is often added to the mixture as a diluting agent to control the ratio between chemical etching and physical sputtering. The most popular mixtures to etch Si are $Cl_2/O_2/Ar$, CF_4/O_2, SF_6/O_2 and (He/)H_2/HBr, or a combination.[14-21]. Indeed, the shift towards more complex gas mixtures for smaller device etching is clearly visible. While in the early days, a relatively simple mixture of Cl_2/O_2(/Ar) was sufficient to etch Si with the desired resolution, nowadays more gases are typically added to the mixture and complex mixtures like $CF_4/CHF_3/H_2/Cl_2/O_2$/HBr and other combinations have been applied for this purpose.[22]

However, mixing gases or changing the fraction of a gas can sometimes yield unwanted reaction products or unexpected changes in the overall plasma properties due to the increased complexity of the system. The goal of this work is therefore to achieve a better insight in the gas phase (i.e., bulk plasma) chemistry for different gas ratios and to elucidate how the components of the mixture influence the overall plasma properties. A computational approach is most suitable for this purpose because we can study in detail the underlying chemical reactions responsible for the observed changes.

II. Computational details

To study the gas phase chemistry of a low-pressure high-density $CF_4/CHF_3/H_2/Cl_2/O_2$/HBr plasma, we apply the hybrid plasma equipment model (HPEM), developed by Kushner.[23] This model calculates the plasma characteristics by combining a Monte Carlo method for the electrons and a fluid simulation for the heavy plasma species. A more detailed explanation of the model can be found in this reference.[23] Reaction sets for pure CF_4, CHF_3, H_2, Cl_2, O_2 and HBr have been established

before.[24-29] Moreover, reaction sets for relatively simple mixtures like $Ar/Cl_2/O_2$ and CF_4/O_2 have also been constructed in previous work.[14,15]

However, establishing a proper reaction set when mixing all different gases is not obvious. Due to the extensive list of different species, the number of reactions between all these species grows nearly exponentially. Indeed, all cross-products between oxygen, fluorine, carbon, hydrogen, chlorine and bromine have to be considered, like CO_xF_y, CH_xO_y, etc., which yields an extremely large, if not unlimited, number of possible products. As a solution, the number of reaction cross-products included in the simulation is typically limited by two factors: (i) the importance or density of the species in the plasma and (ii) the available data (i.e., cross sections and reaction rate coefficients) for properly modelling the gas phase chemistry. For example, in our previous work, various products between chlorine and oxygen have been considered, like ClO, Cl_2O, Cl_2O_2, etc., and it was found that, under typical wafer processing conditions, the densities of all these products are negligible except for ClO.[14] Indeed, all other products have concentrations in the ppm-range or lower, so they will not have a significant contribution to the overall plasma characteristics. In this case, it is allowed, and even advised in terms of calculation time, to exclude these species from the reaction set, as the overall plasma properties will not change significantly when these species are included or not. Reaction products with very low densities should therefore only be considered if specific information on those products is desired. If it is unknown whether a product will have a significant density, it is advised to include it in the reaction set (if sufficient data is available) and check its density by performing some quick tests.

The density of a reaction cross-product is dependent on the stability of the species, and the reaction path to form that species. For example, stable products like H_2O, CO_2, HCl are likely to be present in a plasma containing H, O and Cl, because these products are energetically favored and are easily formed in one or two reactions. In a CF_4/H_2 plasma, it is likely to create CH_x species or even C_xH_y (where $x > 1$). However, since these mixtures are typically applied in low-pressure high-density plasmas, the plasma is usually in a dissociative regime, so it is more likely to dissociate products than to form larger molecules. Indeed, dusty plasmas, where species can accumulate in the gas phase, typically occur at higher pressures.[30]

Table 1 gives an overview of the 65 species included in our model for the $CF_4/CHF_3/H_2/Cl_2/O_2/HBr$ plasma. The reaction cross-products considered are HF, COF_2, COF, FO, CO_2, CO, H_2O, OH, HCl and ClO, as shown in **Table 1**.

Table 1. Overview of the 65 species included in the $CF_4/CHF_3/H_2/Cl_2/O_2/HBr$ reaction set.

Neutral species:	CF_4, CF_3, CF_2, CF, C, F_2, F, F*, CHF_3, CHF_2, CHF, CH, CH_2, H_2, H, O_2, O, O*, Cl_2, Cl, Cl*, HBr, HBr*, Br, Br*, HF, COF_2, COF, FO, CO_2, CO, H_2O, OH, HCl, ClO
Charged species:	CF_3^+, CF_3^-, CF_2^+, CF^+, C^+, F_2^+, F^+, F^-, CHF_2^+, CHF^+, CH^+, CH_2^+, H_2^+, H^+, H_3^+, O_2^+, O^+, O^-, Cl_2^+, Cl^+, Cl^-, HBr^+, Br^+, Br^-, CO_2^+, CO^+, H_2O^+, HCl^+, ClO^+, electrons

The electron impact reactions included in the model are listed in **Table 2**. Most electron impact reactions are described by an energy-dependent cross section, which can be found in the corresponding reference of **Table 2.** Some reactions are described with a rate coefficient, as presented by the formulas in **Table 2**. Also the threshold electron energy is shown for each electron impact reaction, which gives some insight in which reactions occur more easily at typical plasma etch conditions. Note that three different vibrational levels of HBr are included, but they are all denoted as HBr*. Nevertheless, they are characterized by three different threshold energies, as indicated in the Table (i.e., 0.3/0.6/0.9 eV). Likewise, the reactions of these vibrational levels are also characterized by three different threshold energies in the Table.

Table 2. Electron impact reactions included in the model. The rate of each reaction is defined by an electron energy dependent cross section σ(E), which can be found in the corresponding reference, or by a rate coefficient included in the table, where T_e is the absolute value of the electron temperature in eV. The threshold energy of each reaction is also shown. Elastic collisions are included in the model but not listed in the Table.

Electron impact reaction	Cross section σ(E) or rate coefficient	Threshold energy	Reference
$e + CF_4 \rightarrow CF_3 + F^-$	σ(E)	3.00 eV	[31]
$e + CF_4 \rightarrow CF_3^- + F$	σ(E)	4.00 eV	[31]
$e + CF_4 \rightarrow CF_3 + F + e$	σ(E)	12.00 eV	[31]
$e + CF_4 \rightarrow CF_2 + F + F + e$	σ(E)	14.00 eV	[31]
$e + CF_4 \rightarrow CF + F + F_2 + e$	σ(E)	18.00 eV	[31]
$e + CF_4 \rightarrow CF_3^+ + F^- + e$	σ(E)	11.00 eV	[31]
$e + CF_4 \rightarrow CF_3^+ + F + 2e$	σ(E)	16.25 eV	[31]
$e + CF_4 \rightarrow CF_3^+ + F^+ + 3e$	σ(E)	35.00 eV	[31]

$e + CF_4 \rightarrow CF_2^+ + F + F + 2e$	σ(E)	20.00 eV	[31]
$e + CF_4 \rightarrow CF^+ + F + F_2 + 2e$	σ(E)	25.00 eV	[31]
$e + CF_4 \rightarrow CF_3 + F^+ + 2e$	σ(E)	30.00 eV	[31]
$e + CF_3 \rightarrow CF_2 + F^-$	σ(E)	4.40 eV	[31]
$e + CF_3 \rightarrow CF_2 + F + e$	σ(E)	7.70 eV	[31]
$e + CF_3 \rightarrow CF_3^+ + 2e$	σ(E)	8.90 eV	[31]
$e + CF_3 \rightarrow CF_2^+ + F + 2e$	σ(E)	17.00 eV	[31]
$e + CF_3 \rightarrow CF^+ + F + F + 2e$	σ(E)	20.00 eV	[31]
$e + CF_3 \rightarrow CF_2 + F^+ + 2e$	σ(E)	20.00 eV	[31]
$e + CF_2 \rightarrow CF + F^-$	σ(E)	4.40 eV	[31]
$e + CF_2 \rightarrow CF + F + e$	σ(E)	8.70 eV	[31]
$e + CF_2 \rightarrow CF_2^+ + 2e$	σ(E)	11.00 eV	[31]
$e + CF_2 \rightarrow CF^+ + F + 2e$	σ(E)	14.00 eV	[31]
$e + CF_2 \rightarrow CF + F^+ + 2e$	σ(E)	30.00 eV	[31]
$e + CF \rightarrow C + F + e$	σ(E)	5.60 eV	[32]
$e + CF \rightarrow CF^+ + 2e$	σ(E)	10.38 eV	[33]
$e + C \rightarrow C^+ + 2e$	σ(E)	11.26 eV	[33]
$e + CF_3^+ \rightarrow CF_2 + F$	σ(E)	0.00 eV	[34]
$e + CF_2^+ \rightarrow CF + F$	σ(E)	0.00 eV	[34]
$e + F_2 \rightarrow F + F^-$	σ(E)	0.00 eV	[34]
$e + F_2 \rightarrow F + F + e$	σ(E)	3.16 eV	[34]
$e + F_2 \rightarrow F_2^+ + 2e$	σ(E)	15.69 eV	[34]
$e + F_2^+ \rightarrow F + F$	σ(E)	0.00 eV	[34]
$e + F \rightarrow F^* + e$	σ(E)	12.70 eV	[35]
$e + F \rightarrow F^* + e$	σ(E)	12.99 eV	[35]
$e + F \rightarrow F^+ + 2e$	σ(E)	17.42 eV	[35]
$e + F^* \rightarrow F + e$	σ(E)	0.00 eV	[35]
$e + F^* \rightarrow F^+ + 2e$	σ(E)	4.72 eV	[36]
$e + CHF_3 \rightarrow CHF_2 + F^-$	σ(E)	0.05 eV	[37]
$e + CHF_3 \rightarrow CHF_2 + F + e$	σ(E)	13.00 eV	[37]
$e + CHF_3 \rightarrow CHF_2 + F^+ + 2e$	σ(E)	37.00 eV	[37]
$e + CHF_3 \rightarrow CHF_2^+ + F + 2e$	σ(E)	16.80 eV	[37]
$e + CHF_3 \rightarrow CHF_2^+ + F^- + e$	σ(E)	11.50 eV	[37]
$e + CHF_3 \rightarrow CHF + F + F + e$	σ(E)	35.00 eV	[37]
$e + CHF_3 \rightarrow CHF^+ + F + F + 2e$	σ(E)	19.80 eV	[37]
$e + CHF_3 \rightarrow CH^+ + F + F_2 + 2e$	σ(E)	33.50 eV	[37]
$e + CHF_3 \rightarrow CF_3 + H + e$	σ(E)	11.00 eV	[37]
$e + CHF_3 \rightarrow CF_2 + F + H + e$	σ(E)	23.60 eV	[37]
$e + CHF_3 \rightarrow CF + H + F + F + e$	σ(E)	19.50 eV	[37]
$e + CHF_3 \rightarrow CF_3^+ + H + 2e$	σ(E)	15.20 eV	[37]
$e + CHF_3 \rightarrow CF_2^+ + HF + 2e$	σ(E)	17.60 eV	[37]
$e + CHF_3 \rightarrow CF^+ + HF + F + 2e$	σ(E)	20.90 eV	[37]
$e + CHF_2 \rightarrow CHF + F^-$	σ(E)	4.40 eV	Adopted from [37]
$e + CHF_2 \rightarrow CHF + F + e$	σ(E)	7.70 eV	Adopted from [37]
$e + CHF_2 \rightarrow CHF_2^+ + 2e$	σ(E)	8.90 eV	Adopted from [37]
$e + CHF_2 \rightarrow CHF^+ + F + 2e$	σ(E)	17.00 eV	Adopted from [37]
$e + CHF_2 \rightarrow CH^+ + F + F + 2e$	σ(E)	20.00 eV	Adopted from [37]
$e + CHF_2 \rightarrow CHF + F^+ + 2e$	σ(E)	20.00 eV	Adopted from [37]
$e + CHF_2 \rightarrow CF_2 + H + e$	σ(E)	11.00 eV	Adopted from [37]
$e + CHF_2 \rightarrow CF + F + H + e$	σ(E)	23.60 eV	Adopted from [37]
$e + CHF_2 \rightarrow C + H + F + F + e$	σ(E)	19.50 eV	Adopted from [37]
$e + CHF_2 \rightarrow CF_2^+ + H + 2e$	σ(E)	15.20 eV	Adopted from [37]
$e + CHF_2 \rightarrow CF^+ + HF + 2e$	σ(E)	17.60 eV	Adopted from [37]
$e + CHF \rightarrow CH + F^-$	σ(E)	4.40 eV	Adopted from [37]
$e + CHF \rightarrow CH + F + e$	σ(E)	8.70 eV	Adopted from [37]
$e + CHF \rightarrow CHF^+ + 2e$	σ(E)	11.00 eV	Adopted from [37]
$e + CHF \rightarrow CH^+ + F + 2e$	σ(E)	14.00 eV	Adopted from [37]
$e + CHF \rightarrow CH + F^+ + 2e$	σ(E)	30.00 eV	Adopted from [37]
$e + CHF \rightarrow CF + H + e$	σ(E)	11.00 eV	Adopted from [37]
$e + CHF \rightarrow C + F + H + e$	σ(E)	23.60 eV	Adopted from [37]
$e + CHF \rightarrow CF^+ + H + 2e$	σ(E)	15.20 eV	Adopted from [37]

$e + CH \rightarrow C + H + e$	σ(E)	8.50 eV	[38]
$e + CH \rightarrow CH^+ + 2e$	σ(E)	11.3 eV	[38]
$e + CH \rightarrow C^+ + H + 2e$	σ(E)	14.8 eV	[38]
$e + CH^+ \rightarrow C + H$	$3.23 \times 10^{-8} T_e^{-0.42}$ cm^3 s^{-1}	0.00 eV	[38]
$e + CH_2 \rightarrow CH^+ + H + 2e$	σ(E)	7.00 eV	[38]
$e + CH_2 \rightarrow CH + H + e$	σ(E)	10.40 eV	[38]
$e + CH_2 \rightarrow CH_2^+ + 2e$	σ(E)	15.53 eV	[38]
$e + CH_2 \rightarrow C^+ + H_2 + 2e$	σ(E)	17.10 eV	[38]
$e + CH_2^+ \rightarrow CH + H$	$1.88 \times 10^{-8} T_e^{-0.5}$ cm^3 s^{-1}	0.00 eV	[38]
$e + CH_2^+ \rightarrow C + H_2$	$4.82 \times 10^{-9} T_e^{-0.5}$ cm^3 s^{-1}	0.00 eV	[38]
$e + CH_2^+ \rightarrow C + H + H$	$2.35 \times 10^{-8} T_e^{-0.5}$ cm^3 s^{-1}	0.00 eV	[38]
$e + H_2 \rightarrow H + H + e$	σ(E)	8.80 eV	[39]
$e + H_2 \rightarrow H_2^+ + 2e$	σ(E)	15.43 eV	[40]
$e + H_2^+ \rightarrow H^+ + H + e$	σ(E)	0.00 eV	[41]
$e + H_2^+ \rightarrow H + H$	σ(E)	0.00 eV	[41]
$e + H \rightarrow H^+ + 2e$	σ(E)	13.56 eV	[42]
$e + H_3^+ \rightarrow H^+ + H_2 + e$	σ(E)	14.90 eV	[41]
$e + H_3^+ \rightarrow H + H_2$	σ(E)	0.00 eV	[41]
$e + O_2 \rightarrow O^- + O$	σ(E)	0.00 eV	[43]
$e + O_2 \rightarrow O + O + e$	σ(E)	4.50 eV	[43]
$e + O_2 \rightarrow O^* + O + e$	σ(E)	6.00 eV	[43]
$e + O_2 \rightarrow O_2^+ + 2e$	σ(E)	12.06 eV	[43]
$e + O_2 \rightarrow O + O^+ + 2e$	σ(E)	17.00 eV	[43]
$e + O_2^+ \rightarrow O + O$	$1.20 \times 10^{-9} T_e^{-0.7}$ cm^3 s^{-1}	6.88 eV	[43]
$e + O_2^+ \rightarrow O^* + O$	$8.88 \times 10^{-9} T_e^{-0.7}$ cm^3 s^{-1}	4.91 eV	[43]
$e + O^- \rightarrow O + 2e$	$1.95 \times 10^{-11} T_e^{0.5} e^{(-3.4/Te)}$ cm^3 s^{-1}	3.40 eV	[43]
$e + O \rightarrow O^* + e$	σ(E)	1.97 eV	[43]
$e + O \rightarrow O^+ + 2e$	σ(E)	13.62 eV	[43]
$e + O^* \rightarrow O + e$	σ(E)	0.00 eV	[43]
$e + O^* \rightarrow O^+ + 2e$	σ(E)	11.65 eV	[43]
$e + Cl_2 \rightarrow Cl + Cl^-$	σ(E)	0.00 eV	[44]
$e + Cl_2 \rightarrow Cl + Cl + e$	σ(E)	3.12 eV	[44]
$e + Cl_2 \rightarrow Cl_2^+ + 2e$	σ(E)	11.47 eV	[44]
$e + Cl_2^+ \rightarrow Cl + Cl$	$1.00 \times 10^{-7} T_e^{-0.5}$ cm^3 s^{-1}	9.00 eV	[44]
$e + Cl \rightarrow Cl^* + e$	σ(E)	8.90 eV	[44]
$e + Cl \rightarrow Cl^+ + 2e$	σ(E)	12.98 eV	[44]
$e + Cl^* \rightarrow Cl^+ + 2e$	σ(E)	4.09 eV	[44]
$e + Cl^- \rightarrow Cl + 2e$	σ(E)	3.61 eV	[44]
$e + HBr \rightarrow HBr^* + e$	σ(E)	0.3/0.6/0.9 eV	[45]
$e + HBr \rightarrow Br + H + e$	σ(E)	4.34 eV	[23]
$e + HBr \rightarrow Br + H + e$	σ(E)	4.34 eV	[23]
$e + HBr \rightarrow Br^- + H$	σ(E)	0.08 eV	[23]
$e + HBr \rightarrow HBr^+ + 2e$	σ(E)	12.74 eV	[23]
$e + HBr^* \rightarrow HBr + e$	σ(E)	-0.3/0.6/0.9 eV	[45]
$e + HBr^* \rightarrow Br + H + e$	σ(E)	6.6/4.3/9.3 eV	[45]
$e + HBr^* \rightarrow Br^- + H$	σ(E)	6.6/4.3/9.3 eV	[45]
$e + HBr^* \rightarrow HBr^+ + 2e$	σ(E)	6.6/4.3/9.3 eV	[45]
$e + HBr^+ \rightarrow Br + H$	σ(E)	0.00 eV	[23]
$e + Br \rightarrow Br^* + e$	σ(E)	8.90 eV	[23]
$e + Br \rightarrow Br^+ + 2e$	σ(E)	12.99 eV	[23]
$e + Br^* \rightarrow Br^+ + 2e$	σ(E)	4.09 eV	[23]
$e + Br^- \rightarrow Br + 2e$	σ(E)	3.61 eV	[23]
$e + COF_2 \rightarrow COF + F + e$	σ(E)	12.00 eV	Adopted from [31]
$e + CO_2 \rightarrow CO + O^-$	σ(E)	3.85 eV	[46]
$e + CO_2 \rightarrow CO_2^+ + 2e$	σ(E)	13.30 eV	[46]
$e + CO_2^+ \rightarrow CO + O$	σ(E)	0.00 eV	[46]
$e + CO \rightarrow C + O + e$	σ(E)	12.96 eV	[46]
$e + CO \rightarrow CO^+ + 2e$	σ(E)	14.03 eV	[46]
$e + CO \rightarrow C^+ + O + 2e$	σ(E)	21.86 eV	[46]
$e + CO \rightarrow C + O^+ + 2e$	σ(E)	23.79 eV	[46]
$e + H_2O \rightarrow O^- + H_2$	σ(E)	5.53 eV	[47]

$e + H_2O \rightarrow H_2O^+ + 2e$	σ(E)	13.50 eV	[47]
$e + HCl \rightarrow Cl^- + H$	σ(E)	0.75 eV	[48]
$e + HCl \rightarrow Cl + H + e$	σ(E)	2.50 eV	[48]
$e + HCl \rightarrow HCl^+ + 2e$	σ(E)	12.74 eV	[48]
$e + HCl^+ \rightarrow Cl + H$	σ(E)	0.00 eV	[48]
$e + ClO \rightarrow Cl + O + e$	$1.27 \times 10^{-7}\ T_e^{-1.36}\ e^{(-6.84/Te)}\ cm^3\ s^{-1}$	6.84 eV	[49]
$e + ClO \rightarrow ClO^+ + 2e$	$9.48 \times 10^{-9}\ T_e^{0.85}\ e^{(-12.24/Te)}\ cm^3\ s^{-1}$	12.24 eV	[49]

The reactions between all heavy plasma species are listed in **Table 3**. The rate coefficients of most of these reactions can be considered constant in the gas temperature range obtained for the high-density low-pressure plasmas under study (i.e. 300-800 K), hence the rate coefficient is a constant in most cases. If a temperature dependent rate coefficient is available from literature, it is stated as a formula in the table. Due to the large number of different species, the number of heavy particle reactions can be extensive. However, the complete reaction set can be subdivided into three main reaction types: (i) ion-ion neutralizations, (ii) charge transfer reactions and (iii) chemical reactions.

A positive-negative ion-ion recombination, or mutual neutralization, is typically very exothermic and the remaining energy released is absorbed by the reaction products so that they obtain a higher temperature (i.e., "hot neutrals") or a higher internal energy (e.g., higher vibrational state), or it can be absorbed by a third body, or released radiatively as a photon. The rate coefficients k of the ion-ion neutralization reactions are dependent on temperature and the type of species that collide, and can be predicted by the following formula constructed by Shuman *et al.*:[50]

$$k = 3.3\ x\ 10^{-7} \mu^{-0.5} EBE^{-0.24}$$

where μ is the reduced mass of the colliding species, and EBE is the electron binding energy of the anion (in eV). This formula is most suitable for polyatomic ions. The reaction rate coefficient predicted by this formula is typically about one order of magnitude too high for collisions of two monoatomic ions. In these cases, we have thus used the formula to obtain the rate coefficient, but we lowered the coefficient with one order of magnitude, as suggested based on the reference.[50]

The second type of reaction, i.e., a charge transfer reaction between a charged and a neutral species, is more likely if the resulting cation has a lower electron binding energy than the cation before reaction. For example, it is more likely that charge transfer occurs from $F^+ + Cl$ to $Cl^+ + F$ than in the opposite direction, because F is more electronegative than Cl. We took this into account when

constructing our reaction set. Unfortunately, little data is available on charge transfer reaction rate constants and we therefore had to estimate a large number of coefficients in the list. However, it is common knowledge that charge transfer reaction rate coefficients for these chemistries typically have values between 10^{-9} and 10^{-11} cm^3 s^{-1}. We therefore have defined a coefficient of 5 x 10^{-10} cm^3 s^{-1} for the reactions of which no data is available in literature. In principle, charge transfer rate coefficients are dependent on the type of reactants and their ionization energies, thus the rate coefficient will be slightly different for each different combination of reactants, but they are all well estimated around 10^{-10} - 10^{-9} cm^3 s^{-1}.

The third subset in the heavy particle reaction set (**Table 3**) comprises all chemical reactions, or in other words, all reactions where bonds are formed or broken. Similar to the charge transfer reactions, only reactions are considered where the total energy of the products is lower than the total energy of the reactants. For example, the reaction $F + CHF_3 \rightarrow CF_3 + HF$ is more likely to happen in this direction than in the other way, because the bond energy of HF is higher than that of CH in CHF_3. All rate coefficients included in this subset were found in literature, and we made sure that at least one source and loss reaction is considered for each species.

Finally, because we focus on the gas phase chemistry in this paper, we have included a simplified wall reaction set, assuming that neutrals are always reflected from the walls, the ions and excited species are reflected as their neutral ground state counterparts, and the electrons are lost at the walls.

Table 3. Heavy particle reactions included in the model, with corresponding reaction rate coefficients and references where these data were adopted from. Some rate coefficients are defined as gas temperature dependent, where T_{gas} is in Kelvin. Elastic collisions are not included for heavy particle reactions, because these species are treated in the fluid module of the plasma model, hence these reactions are obsolete.

Heavy particle reaction	Rate coefficient (cm^3 s^{-1})	Reference
1. Ion-ion neutralizations		
$CF_3^- + CF_3^+ \rightarrow CF_3 + CF_3$	3.41 x 10^{-8}	[50]
$CF_3^- + CF_2^+ \rightarrow CF_2 + CF_3$	3.72 x 10^{-8}	[50]
$CF_3^- + CF^+ \rightarrow CF + CF_3$	4.33 x 10^{-8}	[50]
$CF_3^- + C^+ \rightarrow C + CF_3$	6.27 x 10^{-8}	[50]
$CF_3^- + F_2^+ \rightarrow F_2 + CF_3$	4.05 x 10^{-8}	[50]
$CF_3^- + F^+ \rightarrow F + CF_3$	5.19 x 10^{-8}	[50]
$CF_3^- + CHF_2^+ \rightarrow CHF_2 + CF_3$	3.70 x 10^{-8}	[50]

$CF_3^- + CHF^+ \rightarrow CHF + CF_3$	4.28×10^{-8}	[50]
$CF_3^- + CH^+ \rightarrow CH + CF_3$	6.06×10^{-8}	[50]
$CF_3^- + CH_2^+ \rightarrow CH_2 + CF_3$	5.87×10^{-8}	[50]
$CF_3^- + H_3^+ \rightarrow H_2 + H + CF_3$	1.18×10^{-7}	[50]
$CF_3^- + H_2^+ \rightarrow H_2 + CF_3$	1.44×10^{-7}	[50]
$CF_3^- + H^+ \rightarrow H + CF_3$	2.02×10^{-7}	[50]
$CF_3^- + O_2^+ \rightarrow O_2 + CF_3$	4.28×10^{-8}	[50]
$CF_3^- + O^+ \rightarrow O + CF_3$	5.56×10^{-8}	[50]
$CF_3^- + Cl_2^+ \rightarrow Cl_2 + CF_3$	3.39×10^{-8}	[50]
$CF_3^- + Cl^+ \rightarrow Cl + CF_3$	4.14×10^{-8}	[50]
$CF_3^- + HBr^+ \rightarrow HBr + CF_3$	3.29×10^{-8}	[50]
$CF_3^- + Br^+ \rightarrow Br + CF_3$	3.30×10^{-8}	[50]
$CF_3^- + CO_2^+ \rightarrow CO_2 + CF_3$	3.87×10^{-8}	[50]
$CF_3^- + CO^+ \rightarrow CO + CF_3$	4.49×10^{-8}	[50]
$CF_3^- + H_2O^+ \rightarrow H_2O + CF_3$	5.30×10^{-8}	[50]
$CF_3^- + HCl^+ \rightarrow HCl + CF_3$	4.10×10^{-8}	[50]
$CF_3^- + ClO^+ \rightarrow ClO + CF_3$	3.69×10^{-8}	[50]
$F^- + CF_3^+ \rightarrow CF_3 + F$	3.41×10^{-8}	[50]
$F^- + CF_2^+ \rightarrow CF_2 + F$	3.72×10^{-8}	[50]
$F^- + CF^+ \rightarrow CF + F$	4.33×10^{-8}	[50]
$F^- + C^+ \rightarrow C + F$	6.27×10^{-9}	[50]
$F^- + F_2^+ \rightarrow F_2 + F$	4.05×10^{-8}	[50]
$F^- + F^+ \rightarrow F + F$	5.19×10^{-9}	[50]
$F^- + CHF_2^+ \rightarrow CHF_2 + F$	3.70×10^{-8}	[50]
$F^- + CHF^+ \rightarrow CHF + F$	4.28×10^{-8}	[50]
$F^- + CH^+ \rightarrow CH + F$	6.06×10^{-8}	[50]
$F^- + CH_2^+ \rightarrow CH_2 + F$	5.87×10^{-8}	[50]
$F^- + H_3^+ \rightarrow H_2 + H + F$	1.18×10^{-7}	[50]
$F^- + H_2^+ \rightarrow H_2 + F$	1.44×10^{-7}	[50]
$F^- + H^+ \rightarrow H + F$	2.02×10^{-8}	[50]
$F^- + O_2^+ \rightarrow O_2 + F$	4.28×10^{-8}	[50]
$F^- + O^+ \rightarrow O + F$	5.56×10^{-9}	[50]
$F^- + Cl_2^+ \rightarrow Cl_2 + F$	3.39×10^{-8}	[50]
$F^- + Cl^+ \rightarrow Cl + F$	4.14×10^{-9}	[50]
$F^- + HBr^+ \rightarrow HBr + F$	3.29×10^{-8}	[50]
$F^- + Br^+ \rightarrow Br + F$	3.30×10^{-9}	[50]
$F^- + CO_2^+ \rightarrow CO_2 + F$	3.87×10^{-8}	[50]
$F^- + CO^+ \rightarrow CO + F$	4.49×10^{-8}	[50]
$F^- + H_2O^+ \rightarrow H_2O + F$	5.30×10^{-8}	[50]
$F^- + HCl^+ \rightarrow HCl + F$	4.10×10^{-8}	[50]
$F^- + ClO^+ \rightarrow ClO + F$	3.69×10^{-8}	[50]
$O^- + CF_3^+ \rightarrow CF_3 + O$	3.41×10^{-8}	[50]
$O^- + CF_2^+ \rightarrow CF_2 + O$	3.72×10^{-8}	[50]
$O^- + CF^+ \rightarrow CF + O$	4.33×10^{-8}	[50]
$O^- + C^+ \rightarrow C + O$	6.27×10^{-9}	[50]
$O^- + F_2^+ \rightarrow F_2 + O$	4.05×10^{-8}	[50]
$O^- + F^+ \rightarrow F + O$	5.19×10^{-9}	[50]
$O^- + CHF_2^+ \rightarrow CHF_2 + O$	3.70×10^{-8}	[50]
$O^- + CHF^+ \rightarrow CHF + O$	4.28×10^{-8}	[50]
$O^- + CH^+ \rightarrow CH + O$	6.06×10^{-8}	[50]
$O^- + CH_2^+ \rightarrow CH_2 + O$	5.87×10^{-8}	[50]
$O^- + H_3^+ \rightarrow H_2 + H + O$	1.18×10^{-7}	[50]
$O^- + H_2^+ \rightarrow H_2 + O$	1.44×10^{-7}	[50]
$O^- + H^+ \rightarrow H + O$	2.02×10^{-8}	[50]
$O^- + O_2^+ \rightarrow O_2 + O$	4.28×10^{-8}	[50]
$O^- + O^+ \rightarrow O + O$	5.56×10^{-9}	[50]
$O^- + Cl_2^+ \rightarrow Cl_2 + O$	3.39×10^{-8}	[50]
$O^- + Cl^+ \rightarrow Cl + O$	4.14×10^{-9}	[50]
$O^- + HBr^+ \rightarrow HBr + O$	3.29×10^{-8}	[50]
$O^- + Br^+ \rightarrow Br + O$	3.30×10^{-9}	[50]
$O^- + CO_2^+ \rightarrow CO_2 + O$	3.87×10^{-8}	[50]

$O^- + CO^+ \rightarrow CO + O$	4.49×10^{-8}	[50]
$O^- + H_2O^+ \rightarrow H_2O + O$	5.30×10^{-8}	[50]
$O^- + HCl^+ \rightarrow HCl + O$	4.10×10^{-8}	[50]
$O^- + ClO^+ \rightarrow ClO + O$	3.69×10^{-8}	[50]
$Cl^- + CF_3^+ \rightarrow CF_3 + Cl$	3.41×10^{-8}	[50]
$Cl^- + CF_2^+ \rightarrow CF_2 + Cl$	3.72×10^{-8}	[50]
$Cl^- + CF^+ \rightarrow CF + Cl$	4.33×10^{-8}	[50]
$Cl^- + C^+ \rightarrow C + Cl$	6.27×10^{-9}	[50]
$Cl^- + F_2^+ \rightarrow F_2 + Cl$	4.05×10^{-8}	[50]
$Cl^- + F^+ \rightarrow F + Cl$	5.19×10^{-9}	[50]
$Cl^- + CHF_2^+ \rightarrow CHF_2 + Cl$	3.70×10^{-8}	[50]
$Cl^- + CHF^+ \rightarrow CHF + Cl$	4.28×10^{-8}	[50]
$Cl^- + CH^+ \rightarrow CH + Cl$	6.06×10^{-8}	[50]
$Cl^- + CH_2^+ \rightarrow CH_2 + Cl$	5.87×10^{-8}	[50]
$Cl^- + H_3^+ \rightarrow H_2 + H + Cl$	1.18×10^{-7}	[50]
$Cl^- + H_2^+ \rightarrow H_2 + Cl$	1.44×10^{-7}	[50]
$Cl^- + H^+ \rightarrow H + Cl$	2.02×10^{-8}	[50]
$Cl^- + O_2^+ \rightarrow O_2 + Cl$	4.28×10^{-8}	[50]
$Cl^- + O^+ \rightarrow O + Cl$	5.56×10^{-9}	[50]
$Cl^- + Cl_2^+ \rightarrow Cl_2 + Cl$	3.39×10^{-8}	[50]
$Cl^- + Cl^+ \rightarrow Cl + Cl$	4.14×10^{-9}	[50]
$Cl^- + HBr^+ \rightarrow HBr + Cl$	3.29×10^{-8}	[50]
$Cl^- + Br^+ \rightarrow Br + Cl$	3.30×10^{-9}	[50]
$Cl^- + CO_2^+ \rightarrow CO_2 + Cl$	3.87×10^{-8}	[50]
$Cl^- + CO^+ \rightarrow CO + Cl$	4.49×10^{-8}	[50]
$Cl^- + H_2O^+ \rightarrow H_2O + Cl$	5.30×10^{-8}	[50]
$Cl^- + HCl^+ \rightarrow HCl + Cl$	4.10×10^{-8}	[50]
$Cl^- + ClO^+ \rightarrow ClO + Cl$	3.69×10^{-8}	[50]
$Br^- + CF_3^+ \rightarrow CF_3 + Br$	3.41×10^{-8}	[50]
$Br^- + CF_2^+ \rightarrow CF_2 + Br$	3.72×10^{-8}	[50]
$Br^- + CF^+ \rightarrow CF + Br$	4.33×10^{-8}	[50]
$Br^- + C^+ \rightarrow C + Br$	6.27×10^{-9}	[50]
$Br^- + F_2^+ \rightarrow F_2 + Br$	4.05×10^{-8}	[50]
$Br^- + F^+ \rightarrow F + Br$	5.19×10^{-9}	[50]
$Br^- + CHF_2^+ \rightarrow CHF_2 + Br$	3.70×10^{-8}	[50]
$Br^- + CHF^+ \rightarrow CHF + Br$	4.28×10^{-8}	[50]
$Br^- + CH^+ \rightarrow CH + Br$	6.06×10^{-8}	[50]
$Br^- + CH_2^+ \rightarrow CH_2 + Br$	5.87×10^{-8}	[50]
$Br^- + H_3^+ \rightarrow H_2 + H + Br$	1.18×10^{-7}	[50]
$Br^- + H_2^+ \rightarrow H_2 + Br$	1.44×10^{-7}	[50]
$Br^- + H^+ \rightarrow H + Br$	2.02×10^{-8}	[50]
$Br^- + O_2^+ \rightarrow O_2 + Br$	4.28×10^{-8}	[50]
$Br^- + O^+ \rightarrow O + Br$	5.56×10^{-9}	[50]
$Br^- + Cl_2^+ \rightarrow Cl_2 + Br$	3.39×10^{-8}	[50]
$Br^- + Cl^+ \rightarrow Cl + Br$	4.14×10^{-9}	[50]
$Br^- + HBr^+ \rightarrow HBr + Br$	3.29×10^{-8}	[50]
$Br^- + Br^+ \rightarrow Br + Br$	3.30×10^{-9}	[50]
$Br^- + CO_2^+ \rightarrow CO_2 + Br$	3.87×10^{-8}	[50]
$Br^- + CO^+ \rightarrow CO + Br$	4.49×10^{-8}	[50]
$Br^- + H_2O^+ \rightarrow H_2O + Br$	5.30×10^{-8}	[50]
$Br^- + HCl^+ \rightarrow HCl + Br$	4.10×10^{-8}	[50]
$Br^- + ClO^+ \rightarrow ClO + Br$	3.69×10^{-8}	[50]

2. Charge transfer reactions

$F^+ + CF_4 \rightarrow CF_3^+ + F_2$	1.00×10^{-9}	[51]
$F^+ + CF_3 \rightarrow CF_2^+ + F_2$	1.09×10^{-9}	[51]
$F^+ + CF_2 \rightarrow CF^+ + F_2$	2.28×10^{-9}	[51]
$F^+ + CF \rightarrow CF^+ + F$	5.00×10^{-10}	[51]
$F^+ + C \rightarrow C^+ + F$	5.00×10^{-10}	[51]
$F^+ + F_2 \rightarrow F_2^+ + F$	7.94×10^{-10}	[51]
$F^+ + CHF_2 \rightarrow CHF_2^+ + F$	5×10^{-10}	estimated

$F^+ + CHF \rightarrow CHF^+ + F$	5×10^{-10}	estimated
$F^+ + CH \rightarrow CH^+ + F$	5×10^{-10}	estimated
$F^+ + CH_2 \rightarrow CH_2^+ + F$	5×10^{-10}	estimated
$F^+ + H_2 \rightarrow H_2^+ + F$	5×10^{-10}	estimated
$F^+ + H \rightarrow H^+ + F$	5×10^{-10}	estimated
$F^+ + O_2 \rightarrow O_2^+ + F$	7.14×10^{-10}	[52]
$F^+ + O_2 \rightarrow O^+ + FO$	5.04×10^{-11}	[52]
$F^+ + O \rightarrow O^+ + F$	1.00×10^{-10}	[52]
$F^+ + Cl_2 \rightarrow Cl_2^+ + F$	5×10^{-10}	estimated
$F^+ + Cl \rightarrow Cl^+ + F$	5×10^{-10}	estimated
$F^+ + HBr \rightarrow HBr^+ + F$	5×10^{-10}	estimated
$F^+ + Br \rightarrow Br^+ + F$	5×10^{-10}	estimated
$F^+ + CO_2 \rightarrow CO_2^+ + F$	5×10^{-10}	estimated
$F^+ + CO \rightarrow CO^+ + F$	5×10^{-10}	estimated
$F^+ + H_2O \rightarrow H_2O^+ + F$	5×10^{-10}	estimated
$F^+ + HCl \rightarrow HCl^+ + F$	5×10^{-10}	estimated
$F^+ + ClO \rightarrow ClO^+ + F$	5×10^{-10}	estimated
$H_3^+ + CF_3 \rightarrow CF_3^+ + H_2 + H$	5×10^{-10}	estimated
$H_3^+ + CF_2 \rightarrow CF_2^+ + H_2 + H$	5×10^{-10}	estimated
$H_3^+ + CF \rightarrow CF^+ + H_2 + H$	5×10^{-10}	estimated
$H_3^+ + C \rightarrow CH^+ + H_2$	2.00×10^{-9}	[53]
$H_3^+ + F_2 \rightarrow F_2^+ + H_2 + H$	5×10^{-10}	estimated
$H_3^+ + CHF_2 \rightarrow CHF_2^+ + H_2 + H$	5×10^{-10}	estimated
$H_3^+ + CHF \rightarrow CHF^+ + H_2 + H$	5×10^{-10}	estimated
$H_3^+ + CH \rightarrow CH_2^+ + H_2$	1.20×10^{-9}	estimated
$H_3^+ + CH_2 \rightarrow CH_2^+ + H_2 + H$	5×10^{-10}	estimated
$H_3^+ + H_2 \rightarrow H_2^+ + H_2 + H$	5×10^{-10}	estimated
$H_3^+ + H \rightarrow H^+ + H_2 + H$	5×10^{-10}	estimated
$H_3^+ + O_2 \rightarrow O_2^+ + H_2 + H$	5×10^{-10}	estimated
$H_3^+ + O \rightarrow O^+ + H_2 + H$	5×10^{-10}	estimated
$H_3^+ + Cl_2 \rightarrow Cl_2^+ + H_2 + H$	5×10^{-10}	estimated
$H_3^+ + Cl \rightarrow Cl^+ + H_2 + H$	5×10^{-10}	estimated
$H_3^+ + HBr \rightarrow HBr^+ + H_2 + H$	5×10^{-10}	estimated
$H_3^+ + Br \rightarrow Br^+ + H_2 + H$	5×10^{-10}	estimated
$H_3^+ + CO_2 \rightarrow CO_2^+ + H_2 + H$	5×10^{-10}	estimated
$H_3^+ + CO \rightarrow CO^+ + H_2 + H$	5×10^{-10}	estimated
$H_3^+ + H_2O \rightarrow H_2O^+ + H_2 + H$	5×10^{-10}	estimated
$H_3^+ + HCl \rightarrow HCl^+ + H_2 + H$	5×10^{-10}	estimated
$H_3^+ + ClO \rightarrow ClO^+ + H_2 + H$	5×10^{-10}	estimated
$F_2^+ + CF_4 \rightarrow CF_3^+ + F + F_2$	1.00×10^{-10}	[51]
$F_2^+ + CF_3 \rightarrow CF_3^+ + F + F$	1.60×10^{-9}	[51]
$F_2^+ + CF_2 \rightarrow CF_2^+ + F_2$	1.00×10^{-9}	[51]
$F_2^+ + CF_2 \rightarrow CF_3^+ + F$	1.79×10^{-9}	[51]
$F_2^+ + CF \rightarrow CF_2^+ + F$	2.18×10^{-9}	[51]
$F_2^+ + C \rightarrow CF^+ + F$	1.04×10^{-9}	[51]
$F_2^+ + CHF_2 \rightarrow CHF_2^+ + F_2$	5×10^{-10}	estimated
$F_2^+ + CHF \rightarrow CHF^+ + F_2$	5×10^{-10}	estimated
$F_2^+ + CH \rightarrow CH^+ + F_2$	5×10^{-10}	estimated
$F_2^+ + CH_2 \rightarrow CH_2^+ + F_2$	5×10^{-10}	estimated
$F_2^+ + H_2 \rightarrow H_2^+ + F_2$	5×10^{-10}	estimated
$F_2^+ + H \rightarrow H^+ + F_2$	5×10^{-10}	estimated
$F_2^+ + O_2 \rightarrow O_2^+ + F_2$	5×10^{-10}	estimated
$F_2^+ + O \rightarrow O^+ + F_2$	5×10^{-10}	estimated
$F_2^+ + Cl_2 \rightarrow Cl_2^+ + F_2$	5×10^{-10}	estimated
$F_2^+ + Cl \rightarrow Cl^+ + F_2$	5×10^{-10}	estimated
$F_2^+ + HBr \rightarrow HBr^+ + F_2$	5×10^{-10}	estimated
$F_2^+ + Br \rightarrow Br^+ + F_2$	5×10^{-10}	estimated
$F_2^+ + CO_2 \rightarrow CO_2^+ + F_2$	5×10^{-10}	estimated
$F_2^+ + CO \rightarrow CO^+ + F_2$	5×10^{-10}	estimated
$F_2^+ + H_2O \rightarrow H_2O^+ + F_2$	5×10^{-10}	estimated
$F_2^+ + HCl \rightarrow HCl^+ + F_2$	5×10^{-10}	estimated

$F_2^+ + ClO \rightarrow ClO^+ + F_2$	5×10^{-10}	estimated
$H_2^+ + CF_3 \rightarrow CF_3^+ + H_2$	5×10^{-10}	estimated
$H_2^+ + CF_2 \rightarrow CF_2^+ + H_2$	5×10^{-10}	estimated
$H_2^+ + CF \rightarrow CF^+ + H_2$	5×10^{-10}	estimated
$H_2^+ + C \rightarrow CH^+ + H$	2.40×10^{-9}	[53]
$H_2^+ + CHF_2 \rightarrow CHF_2^+ + H_2$	5×10^{-10}	estimated
$H_2^+ + CHF \rightarrow CHF^+ + H_2$	5×10^{-10}	estimated
$H_2^+ + CH \rightarrow CH_2^+ + H$	7.10×10^{-10}	[53]
$H_2^+ + CH \rightarrow CH^+ + H_2$	7.10×10^{-10}	[53]
$H_2^+ + CH_2 \rightarrow CH_2^+ + H_2$	1.00×10^{-9}	[53]
$H_2^+ + H_2 \rightarrow H_3^+ + H$	$2.00 \times 10^{-9} T_{gas}^{-0.5}$	[54]
$H_2^+ + H \rightarrow H^+ + H_2$	6.40×10^{-10}	[55]
$H_2^+ + O_2 \rightarrow O_2^+ + H_2$	5×10^{-10}	estimated
$H_2^+ + O \rightarrow O^+ + H_2$	5×10^{-10}	estimated
$H_2^+ + Cl_2 \rightarrow Cl_2^+ + H_2$	5×10^{-10}	estimated
$H_2^+ + Cl \rightarrow Cl^+ + H_2$	5×10^{-10}	estimated
$H_2^+ + HBr \rightarrow HBr^+ + H_2$	5×10^{-10}	estimated
$H_2^+ + Br \rightarrow Br^+ + H_2$	5×10^{-10}	estimated
$H_2^+ + CO_2 \rightarrow CO_2^+ + H_2$	5×10^{-10}	estimated
$H_2^+ + CO \rightarrow CO^+ + H_2$	5×10^{-10}	estimated
$H_2^+ + H_2O \rightarrow H_2O^+ + H_2$	5×10^{-10}	estimated
$H_2^+ + HCl \rightarrow HCl^+ + H_2$	5×10^{-10}	estimated
$H_2^+ + ClO \rightarrow ClO^+ + H_2$	5×10^{-10}	estimated
$CO^+ + CF_4 \rightarrow CF_3^+ + COF$	7.00×10^{-10}	[52]
$CO^+ + CF_3 \rightarrow CF_2^+ + COF$	7.00×10^{-10}	[52]
$CO^+ + CF_2 \rightarrow CF^+ + COF$	7.00×10^{-10}	[52]
$CO^+ + CF \rightarrow CF^+ + CO$	5×10^{-10}	estimated
$CO^+ + C \rightarrow C^+ + CO$	5×10^{-10}	estimated
$CO^+ + CHF_2 \rightarrow CHF_2^+ + CO$	5×10^{-10}	estimated
$CO^+ + CHF \rightarrow CHF^+ + CO$	5×10^{-10}	estimated
$CO^+ + CH \rightarrow CH^+ + CO$	5×10^{-10}	estimated
$CO^+ + CH_2 \rightarrow CH_2^+ + CO$	5×10^{-10}	estimated
$CO^+ + H \rightarrow H^+ + CO$	5×10^{-10}	estimated
$CO^+ + O_2 \rightarrow O_2^+ + CO$	1.20×10^{-10}	[52]
$CO^+ + O \rightarrow O^+ + CO$	1.40×10^{-10}	[52]
$CO^+ + Cl_2 \rightarrow Cl_2^+ + CO$	5×10^{-10}	estimated
$CO^+ + Cl \rightarrow Cl^+ + CO$	5×10^{-10}	estimated
$CO^+ + HBr \rightarrow HBr^+ + CO$	5×10^{-10}	estimated
$CO^+ + Br \rightarrow Br^+ + CO$	5×10^{-10}	estimated
$CO^+ + CO_2 \rightarrow CO_2^+ + CO$	5×10^{-10}	estimated
$CO^+ + H_2O \rightarrow H_2O^+ + CO$	5×10^{-10}	estimated
$CO^+ + HCl \rightarrow HCl^+ + CO$	5×10^{-10}	estimated
$CO^+ + ClO \rightarrow ClO^+ + CO$	5×10^{-10}	estimated
$O^+ + CF_4 \rightarrow CF_3^+ + FO$	1.40×10^{-9}	[52]
$O^+ + CF_3 \rightarrow CF_3^+ + O$	5×10^{-10}	estimated
$O^+ + CF_2 \rightarrow CF_2^+ + O$	5×10^{-10}	estimated
$O^+ + CF \rightarrow CF^+ + O$	5×10^{-10}	estimated
$O^+ + C \rightarrow C^+ + O$	5×10^{-10}	estimated
$O^+ + CHF_2 \rightarrow CHF_2^+ + O$	5×10^{-10}	estimated
$O^+ + CHF \rightarrow CHF^+ + O$	5×10^{-10}	estimated
$O^+ + CH \rightarrow CH^+ + O$	5×10^{-10}	estimated
$O^+ + CH_2 \rightarrow CH_2^+ + O$	5×10^{-10}	estimated
$O^+ + H \rightarrow H^+ + O$	5×10^{-10}	estimated
$O^+ + O_2 \rightarrow O_2^+ + O$	5×10^{-10}	estimated
$O^+ + Cl_2 \rightarrow Cl_2^+ + O$	1.00×10^{-11}	estimated
$O^+ + Cl \rightarrow Cl^+ + O$	1.00×10^{-11}	estimated
$O^+ + HBr \rightarrow HBr^+ + O$	5×10^{-10}	estimated
$O^+ + Br \rightarrow Br^+ + O$	5×10^{-10}	estimated
$O^+ + CO_2 \rightarrow CO_2^+ + O$	5×10^{-10}	estimated
$O^+ + H_2O \rightarrow H_2O^+ + O$	5×10^{-10}	estimated
$O^+ + HCl \rightarrow HCl^+ + O$	5×10^{-10}	estimated

$O^+ + ClO \rightarrow ClO^+ + O$	4.90×10^{-10}	[49]
$H^+ + CF_3 \rightarrow CF_3^+ + H$	5×10^{-10}	estimated
$H^+ + CF_2 \rightarrow CF_2^+ + H$	5×10^{-10}	estimated
$H^+ + CF \rightarrow CF^+ + H$	5×10^{-10}	estimated
$H^+ + C \rightarrow C^+ + H$	5×10^{-10}	estimated
$H^+ + CHF_2 \rightarrow CHF_2^+ + H$	5×10^{-10}	estimated
$H^+ + CHF \rightarrow CHF^+ + H$	5×10^{-10}	estimated
$H^+ + CH \rightarrow CH^+ + H$	1.90×10^{-9}	[53]
$H^+ + CH_2 \rightarrow CH_2^+ + H$	1.40×10^{-9}	[53]
$H^+ + CH_2 \rightarrow CH^+ + H_2$	1.40×10^{-9}	[53]
$H^+ + O_2 \rightarrow O_2^+ + H$	5×10^{-10}	estimated
$H^+ + Cl_2 \rightarrow Cl_2^+ + H$	5×10^{-10}	estimated
$H^+ + Cl \rightarrow Cl^+ + H$	5×10^{-10}	estimated
$H^+ + HBr \rightarrow HBr^+ + H$	5×10^{-10}	estimated
$H^+ + Br \rightarrow Br^+ + H$	5×10^{-10}	estimated
$H^+ + CO_2 \rightarrow CO_2^+ + H$	5×10^{-10}	estimated
$H^+ + CO \rightarrow CO^+ + H$	5×10^{-10}	estimated
$H^+ + HCl \rightarrow HCl^+ + H$	5×10^{-10}	estimated
$H^+ + ClO \rightarrow ClO^+ + H$	5×10^{-10}	estimated
$H_2O^+ + CF_3 \rightarrow CF_3^+ + H_2O$	5×10^{-10}	estimated
$H_2O^+ + CF_2 \rightarrow CF_2^+ + H_2O$	5×10^{-10}	estimated
$H_2O^+ + CF \rightarrow CF^+ + H_2O$	5×10^{-10}	estimated
$H_2O^+ + C \rightarrow C^+ + H_2O$	5×10^{-10}	estimated
$H_2O^+ + CHF_2 \rightarrow CHF_2^+ + H_2O$	5×10^{-10}	estimated
$H_2O^+ + CHF \rightarrow CHF^+ + H_2O$	5×10^{-10}	estimated
$H_2O^+ + CH \rightarrow CH^+ + H_2O$	5×10^{-10}	estimated
$H_2O^+ + CH_2 \rightarrow CH_2^+ + H_2O$	5×10^{-10}	estimated
$H_2O^+ + O_2 \rightarrow O_2^+ + H_2O$	5×10^{-10}	estimated
$H_2O^+ + Cl_2 \rightarrow Cl_2^+ + H_2O$	5×10^{-10}	estimated
$H_2O^+ + Cl \rightarrow Cl^+ + H_2O$	5×10^{-10}	estimated
$H_2O^+ + HBr \rightarrow HBr^+ + H_2O$	5×10^{-10}	estimated
$H_2O^+ + Br \rightarrow Br^+ + H_2O$	5×10^{-10}	estimated
$H_2O^+ + CO_2 \rightarrow CO_2^+ + H_2O$	5×10^{-10}	estimated
$H_2O^+ + HCl \rightarrow HCl^+ + H_2O$	5×10^{-10}	estimated
$H_2O^+ + ClO \rightarrow ClO^+ + H_2O$	5×10^{-10}	estimated
$CO_2^+ + CF_3 \rightarrow CF_3^+ + CO_2$	5×10^{-10}	estimated
$CO_2^+ + CF_2 \rightarrow CF_2^+ + CO_2$	5×10^{-10}	estimated
$CO_2^+ + CF \rightarrow CF^+ + CO_2$	5×10^{-10}	estimated
$CO_2^+ + C \rightarrow C^+ + CO_2$	5×10^{-10}	estimated
$CO_2^+ + CHF_2 \rightarrow CHF_2^+ + CO_2$	5×10^{-10}	estimated
$CO_2^+ + CHF \rightarrow CHF^+ + CO_2$	5×10^{-10}	estimated
$CO_2^+ + CH \rightarrow CH^+ + CO_2$	5×10^{-10}	estimated
$CO_2^+ + CH_2 \rightarrow CH_2^+ + CO_2$	5×10^{-10}	estimated
$CO_2^+ + O_2 \rightarrow O_2^+ + CO_2$	5×10^{-10}	estimated
$CO_2^+ + Cl_2 \rightarrow Cl_2^+ + CO_2$	5×10^{-10}	estimated
$CO_2^+ + Cl \rightarrow Cl^+ + CO_2$	5×10^{-10}	estimated
$CO_2^+ + HBr \rightarrow HBr^+ + CO_2$	5×10^{-10}	estimated
$CO_2^+ + Br \rightarrow Br^+ + CO_2$	5×10^{-10}	estimated
$CO_2^+ + HCl \rightarrow HCl^+ + CO_2$	5×10^{-10}	estimated
$CO_2^+ + ClO \rightarrow ClO^+ + CO_2$	5×10^{-10}	estimated
$Br^+ + CF_3 \rightarrow CF_3^+ + Br$	5×10^{-10}	estimated
$Br^+ + CF_2 \rightarrow CF_2^+ + Br$	5×10^{-10}	estimated
$Br^+ + CF \rightarrow CF^+ + Br$	5×10^{-10}	estimated
$Br^+ + C \rightarrow C^+ + Br$	5×10^{-10}	estimated
$Br^+ + CHF_2 \rightarrow CHF_2^+ + Br$	5×10^{-10}	estimated
$Br^+ + CHF \rightarrow CHF^+ + Br$	5×10^{-10}	estimated
$Br^+ + CH \rightarrow CH^+ + Br$	5×10^{-10}	estimated
$Br^+ + CH_2 \rightarrow CH_2^+ + Br$	5×10^{-10}	estimated
$Br^+ + O_2 \rightarrow O_2^+ + Br$	5×10^{-10}	estimated
$Br^+ + Cl_2 \rightarrow Cl_2^+ + Br$	5×10^{-10}	estimated
$Br^+ + Cl \rightarrow Cl^+ + Br$	5×10^{-10}	estimated

$Br^+ + HBr \rightarrow HBr^+ + Br$	5×10^{-10}	estimated
$Br^+ + HCl \rightarrow HCl^+ + Br$	5×10^{-10}	estimated
$Br^+ + ClO \rightarrow ClO^+ + Br$	5×10^{-10}	estimated
$Cl^+ + CF_3 \rightarrow CF_3^+ + Cl$	5×10^{-10}	estimated
$Cl^+ + CF_2 \rightarrow CF_2^+ + Cl$	5×10^{-10}	estimated
$Cl^+ + CF \rightarrow CF^+ + Cl$	5×10^{-10}	estimated
$Cl^+ + C \rightarrow C^+ + Cl$	5×10^{-10}	estimated
$Cl^+ + CHF_2 \rightarrow CHF_2^+ + Cl$	5×10^{-10}	estimated
$Cl^+ + CHF \rightarrow CHF^+ + Cl$	5×10^{-10}	estimated
$Cl^+ + CH \rightarrow CH^+ + Cl$	5×10^{-10}	estimated
$Cl^+ + CH_2 \rightarrow CH_2^+ + Cl$	5×10^{-10}	estimated
$Cl^+ + O_2 \rightarrow O_2^+ + Cl$	5×10^{-10}	estimated
$Cl^+ + Cl_2 \rightarrow Cl_2^+ + Cl$	$5.40 \times 10^{-10}\ T_{gas}^{0.5}$	[56]
$Cl^+ + HBr \rightarrow HBr^+ + Cl$	5×10^{-10}	estimated
$Cl^+ + HCl \rightarrow HCl^+ + Cl$	5×10^{-10}	estimated
$Cl^+ + ClO \rightarrow ClO^+ + Cl$	4.90×10^{-10}	estimated
$HCl^+ + CF_3 \rightarrow CF_3^+ + HCl$	5×10^{-10}	estimated
$HCl^+ + CF_2 \rightarrow CF_2^+ + HCl$	5×10^{-10}	estimated
$HCl^+ + CF \rightarrow CF^+ + HCl$	5×10^{-10}	estimated
$HCl^+ + C \rightarrow C^+ + HCl$	5×10^{-10}	estimated
$HCl^+ + CHF_2 \rightarrow CHF_2^+ + HCl$	5×10^{-10}	estimated
$HCl^+ + CHF \rightarrow CHF^+ + HCl$	5×10^{-10}	estimated
$HCl^+ + CH \rightarrow CH^+ + HCl$	5×10^{-10}	estimated
$HCl^+ + CH_2 \rightarrow CH_2^+ + HCl$	5×10^{-10}	estimated
$HCl^+ + O_2 \rightarrow O_2^+ + HCl$	5×10^{-10}	estimated
$HCl^+ + Cl_2 \rightarrow Cl_2^+ + HCl$	5×10^{-10}	estimated
$HCl^+ + HBr \rightarrow HBr^+ + HCl$	5×10^{-10}	estimated
$HCl^+ + ClO \rightarrow ClO^+ + HCl$	5×10^{-10}	estimated
$HBr^+ + CF_3 \rightarrow CF_3^+ + HBr$	5×10^{-10}	estimated
$HBr^+ + CF_2 \rightarrow CF_2^+ + HBr$	5×10^{-10}	estimated
$HBr^+ + CF \rightarrow CF^+ + HBr$	5×10^{-10}	estimated
$HBr^+ + C \rightarrow C^+ + HBr$	5×10^{-10}	estimated
$HBr^+ + CHF_2 \rightarrow CHF_2^+ + HBr$	5×10^{-10}	estimated
$HBr^+ + CHF \rightarrow CHF^+ + HBr$	5×10^{-10}	estimated
$HBr^+ + CH \rightarrow CH^+ + HBr$	5×10^{-10}	estimated
$HBr^+ + CH_2 \rightarrow CH_2^+ + HBr$	5×10^{-10}	estimated
$HBr^+ + O_2 \rightarrow O_2^+ + HBr$	5×10^{-10}	estimated
$HBr^+ + Cl_2 \rightarrow Cl_2^+ + HBr$	5×10^{-10}	estimated
$HBr^+ + ClO \rightarrow ClO^+ + HBr$	5×10^{-10}	estimated
$ClO^+ + CF_3 \rightarrow CF_3^+ + ClO$	5×10^{-10}	estimated
$ClO^+ + CF_2 \rightarrow CF_2^+ + ClO$	5×10^{-10}	estimated
$ClO^+ + CF \rightarrow CF^+ + ClO$	5×10^{-10}	estimated
$ClO^+ + C \rightarrow C^+ + ClO$	5×10^{-10}	estimated
$ClO^+ + CHF_2 \rightarrow CHF_2^+ + ClO$	5×10^{-10}	estimated
$ClO^+ + CHF \rightarrow CHF^+ + ClO$	5×10^{-10}	estimated
$ClO^+ + CH \rightarrow CH^+ + ClO$	5×10^{-10}	estimated
$ClO^+ + CH_2 \rightarrow CH_2^+ + ClO$	5×10^{-10}	estimated
$ClO^+ + O_2 \rightarrow O_2^+ + ClO$	5×10^{-10}	estimated
$ClO^+ + Cl_2 \rightarrow Cl_2^+ + ClO$	5×10^{-10}	estimated
$O_2^+ + CF_3 \rightarrow CF_3^+ + O_2$	5×10^{-10}	estimated
$O_2^+ + CF_2 \rightarrow CF_2^+ + O_2$	5×10^{-10}	estimated
$O_2^+ + CF \rightarrow CF^+ + O_2$	5×10^{-10}	estimated
$O_2^+ + C \rightarrow C^+ + O_2$	5×10^{-10}	estimated
$O_2^+ + CHF_2 \rightarrow CHF_2^+ + O_2$	5×10^{-10}	estimated
$O_2^+ + CHF \rightarrow CHF^+ + O_2$	5×10^{-10}	estimated
$O_2^+ + CH \rightarrow CH^+ + O_2$	5×10^{-10}	estimated
$O_2^+ + CH_2 \rightarrow CH_2^+ + O_2$	5×10^{-10}	estimated
$O_2^+ + Cl_2 \rightarrow Cl_2^+ + O_2$	2.00×10^{-11}	estimated
$Cl_2^+ + CF_3 \rightarrow CF_3^+ + Cl_2$	5×10^{-10}	estimated
$Cl_2^+ + CF_2 \rightarrow CF_2^+ + Cl_2$	5×10^{-10}	estimated
$Cl_2^+ + CF \rightarrow CF^+ + Cl_2$	5×10^{-10}	estimated

$Cl_2^+ + C \rightarrow C^+ + Cl_2$	5×10^{-10}	estimated
$Cl_2^+ + CHF_2 \rightarrow CHF_2^+ + Cl_2$	5×10^{-10}	estimated
$Cl_2^+ + CHF \rightarrow CHF^+ + Cl_2$	5×10^{-10}	estimated
$Cl_2^+ + CH \rightarrow CH^+ + Cl_2$	5×10^{-10}	estimated
$Cl_2^+ + CH_2 \rightarrow CH_2^+ + Cl_2$	5×10^{-10}	estimated
$CH^+ + CF_3 \rightarrow CF_3^+ + CH$	5×10^{-10}	estimated
$CH^+ + CF_2 \rightarrow CF_2^+ + CH$	5×10^{-10}	estimated
$CH^+ + CF \rightarrow CF^+ + CH$	5×10^{-10}	estimated
$CH^+ + C \rightarrow C^+ + CH$	5×10^{-10}	estimated
$CH^+ + H_2 \rightarrow CH_2^+ + H$	1.20×10^{-9}	[53]
$CH^+ + H \rightarrow C^+ + H_2$	7.50×10^{-10}	[53]
$CH^+ + CHF_2 \rightarrow CHF_2^+ + CH$	5×10^{-10}	estimated
$CH^+ + CHF \rightarrow CHF^+ + CH$	5×10^{-10}	estimated
$CH^+ + CH_2 \rightarrow CH_2^+ + CH$	5×10^{-10}	estimated
$C^+ + CF_3 \rightarrow CF_3^+ + C$	5×10^{-10}	estimated
$C^+ + CF_2 \rightarrow CF_2^+ + C$	5×10^{-10}	estimated
$C^+ + CF \rightarrow CF^+ + C$	5×10^{-10}	estimated
$C^+ + CHF_2 \rightarrow CHF_2^+ + C$	5×10^{-10}	estimated
$C^+ + CHF \rightarrow CHF^+ + C$	5×10^{-10}	estimated
$C^+ + CH_2 \rightarrow CH_2^+ + C$	5.20×10^{-10}	[53]
$CHF^+ + CF_3 \rightarrow CF_3^+ + CHF$	5×10^{-10}	estimated
$CHF^+ + CF_2 \rightarrow CF_2^+ + CHF$	5×10^{-10}	estimated
$CHF^+ + CF \rightarrow CF^+ + CHF$	5×10^{-10}	estimated
$CHF^+ + CHF_2 \rightarrow CHF_2^+ + CHF$	5×10^{-10}	estimated
$CHF^+ + CH_2 \rightarrow CH_2^+ + CHF$	5×10^{-10}	estimated
$CF_2^+ + CF_4 \rightarrow CF_3^+ + CF_3$	4.00×10^{-10}	[51]
$CF_2^+ + CF_3 \rightarrow CF_3^+ + CF_2$	1.48×10^{-9}	[51]
$CF_2^+ + CF \rightarrow CF_3^+ + C$	2.06×10^{-9}	[51]
$CF_2^+ + C \rightarrow CF^+ + CF$	1.04×10^{-9}	estimated
$CF_2^+ + CHF_2 \rightarrow CHF_2^+ + CF_2$	5×10^{-10}	estimated
$CF_2^+ + CH_2 \rightarrow CH_2^+ + CF_2$	5×10^{-10}	estimated
$CH_2^+ + CF_3 \rightarrow CF_3^+ + CH_2$	5×10^{-10}	estimated
$CH_2^+ + CF \rightarrow CF^+ + CH_2$	5×10^{-10}	estimated
$CH_2^+ + CHF_2 \rightarrow CHF_2^+ + CH_2$	5×10^{-10}	estimated
$CF^+ + CF_4 \rightarrow CF_3^+ + CF_2$	1.80×10^{-10}	[51]
$CF^+ + CF_3 \rightarrow CF_3^+ + CF$	1.71×10^{-9}	[51]
$CF^+ + CHF_2 \rightarrow CHF_2^+ + CF$	5×10^{-10}	estimated
$CHF_2^+ + CF_3 \rightarrow CF_3^+ + CHF_2$	5×10^{-10}	estimated

3. Chemical reactions

$F + CHF_3 \rightarrow CF_3 + HF$	1.50×10^{-13}	[57]
$F + CHF_2 \rightarrow CF_2 + HF$	5.00×10^{-11}	[57]
$F + CHF \rightarrow CF + HF$	5.00×10^{-11}	[58]
$F + H_2 \rightarrow H + HF$	2.50×10^{-11}	[57]
$H + CHF_3 \rightarrow CF_3 + H_2$	5.20×10^{-19}	[57]
$H + CHF_2 \rightarrow CHF + HF$	1.10×10^{-10}	[57]
$H + CHF_2 \rightarrow CF_2 + H_2$	1.80×10^{-14}	[57]
$H + CHF \rightarrow CH + HF$	4.90×10^{-10}	[57]
$H + CH \rightarrow C + H_2$	1.00×10^{-10}	[59]
$H + CF_3 \rightarrow CF_2 + HF$	9.10×10^{-11}	[57]
$H + CF_2 \rightarrow CF + HF$	4.10×10^{-11}	[57]
$H + CF \rightarrow CH + F$	1.90×10^{-11}	[57]
$H + CF \rightarrow C + HF$	1.91×10^{-11}	[60]
$H + F_2 \rightarrow F + HF$	1.80×10^{-12}	[57]
$CF_3 + CHF_2 \rightarrow CHF_3 + CF_2$	1.70×10^{-12}	[57]
$CH + HF \rightarrow CF + H_2$	5.00×10^{-11}	[57]
$CH_2 + H \rightarrow CH + H_2$	2.01×10^{-10}	[59]
$CH + H_2 \rightarrow CH_2 + H$	6.80×10^{-13}	[59]
$C + H_2 \rightarrow CH + H$	1.50×10^{-10}	[59]
$O^* + CF_4 \rightarrow O + CF_4$	1.80×10^{-13}	[52]
$O^* + COF_2 \rightarrow O + COF_2$	5.30×10^{-11}	[52]

$O^* + COF_2 \rightarrow F_2 + CO_2$	2.10×10^{-11}	[52]
$O^* + CF_3 \rightarrow COF_2 + F$	3.10×10^{-11}	[52]
$O^* + CF_2 \rightarrow COF + F$	1.40×10^{-11}	[52]
$O^* + CF_2 \rightarrow CO + F + F$	4.00×10^{-12}	[52]
$O^* + CF \rightarrow CO + F$	2.00×10^{-11}	[52]
$O^* + COF \rightarrow CO_2 + F$	9.30×10^{-11}	[52]
$O^* + FO \rightarrow O_2 + F$	5.00×10^{-11}	[52]
$O + FO \rightarrow O_2 + F$	2.70×10^{-11}	[52]
$C + O_2 \rightarrow CO + O$	1.60×10^{-11}	[52]
$COF + CF_2 \rightarrow CF_3 + CO$	3.00×10^{-13}	[52]
$COF + CF_2 \rightarrow COF_2 + CF$	3.00×10^{-13}	[52]
$COF + CF_3 \rightarrow CF_4 + CO$	1.00×10^{-11}	[52]
$COF + CF_3 \rightarrow COF_2 + CF_2$	1.00×10^{-11}	[52]
$COF + COF \rightarrow COF_2 + CO$	1.00×10^{-11}	[52]
$O + CF \rightarrow CO + F$	6.60×10^{-11}	[52]
$O + CF_2 \rightarrow COF + F$	3.10×10^{-11}	[52]
$O + CF_2 \rightarrow CO + F + F$	4.00×10^{-12}	[52]
$O + CF_3 \rightarrow COF_2 + F$	3.30×10^{-11}	[52]
$O + COF \rightarrow CO_2 + F$	9.30×10^{-11}	[52]
$O_2 + CF \rightarrow COF + O$	3.30×10^{-11}	[52]
$O + OH \rightarrow H + O_2$	2.40×10^{-11}	[47]
$O^* + H_2O \rightarrow OH + OH$	2.20×10^{-10}	[47]
$OH + H_2 \rightarrow H_2O + H$	7.70×10^{-12}	[47]
$OH + H \rightarrow O + H_2$	1.48×10^{-10}	[61]
$O + H_2 \rightarrow OH + H$	3.44×10^{-10}	[61]
$HCl + H \rightarrow Cl + H_2$	1.48×10^{-10}	estimated based on OH
$Cl + H_2 \rightarrow HCl + H$	3.44×10^{-10}	estimated based on OH
$Cl_2 + O^* \rightarrow ClO + Cl$	2.11×10^{-10}	[49]
$ClO + O \rightarrow O_2 + Cl$	4.11×10^{-11}	[49]
$ClO + Cl \rightarrow Cl_2 + O$	1.27×10^{-12}	[49]
$H + HBr \rightarrow H_2 + Br$	6.50×10^{-12}	[62]

III. Results and Discussion

We consider the following typical operating conditions for wafer processing: 13.56 MHz frequency, 1000 W source power, 40 mTorr gas pressure and 100 sccm total gas flow rate, with a gas mixture of 20% CF_4, 10% CHF_3, 10% H_2, 20% Cl_2, 20% O_2 and 20% HBr. This gas mixing ratio was chosen so that each component is more or less equally present and so that the total fraction of etchant gas(es) is 70%, versus 20% O_2 and 10% H_2, which is a realistic ratio between etching and passivating gases for successful anisotropic etching of Si, although usually even less oxygen is applied to avoid etch stop.[64] The general plasma characteristics of this mixture are discussed in section 1 below. To further investigate the effect of these gas components on the overall plasma chemistry, we will vary the fraction of each chemical component and discuss the results in the subsequent sections. When the fraction of one gas component is varied, the ratio between the other gases is kept constant.

1. General plasma characteristics

The plasma behavior is calculated for a Transformer Coupled Plasma (TCP) reactor with a planar coil on top of the plasma chamber, resembling the LAM Research 2300 Versys Kiyo reactor for etching of 300 mm wafers. The power source (coil) is separated from the plasma by a quartz plate with the gas nozzle in the center of the plate. No bias is applied to the substrate electrode underneath the wafer, as we focus only on the bulk plasma chemistry.

Figures 1(a-f) illustrate the general plasma properties in a two-dimensional half-cross section of the reactor. **Figure 1a** shows the electric field generated by the TCP coil and how it penetrates the plasma chamber. This field is the strongest near the coils and the electrons in the plasma will hence be accelerated most in this area, resulting in a maximum time-average electron temperature of 2.8 eV near the coil as shown in **Figure 1b**. The highest plasma density is also found in the area where the electron temperature is at maximum, since most electron impact ionizations and dissociations occur here. The electron density (**Figure 1c**) and the total ion density (**Figure 1d**) therefore also have a torus shaped maximum following the shape of the coil, and they decrease near the walls due to electron loss and ion neutralization.

The plasma potential profile (**Figure 1e**) correlates to the shape of the plasma density, with a maximum value of 12 V. Similarly, the gas temperature profile (**Figure 1f**) also resembles the shape of the plasma density, although the maximum is slightly further away from the quartz window. Most efficient gas heating processes are electron impact dissociation reactions where hot products (i.e., with high kinetic energy) are created. The gas temperature therefore has a maximum value near 550 K where the plasma density has its maximum, and it decreases towards the walls where the gas temperature becomes equal to the fixed wall temperature of 20 °C.

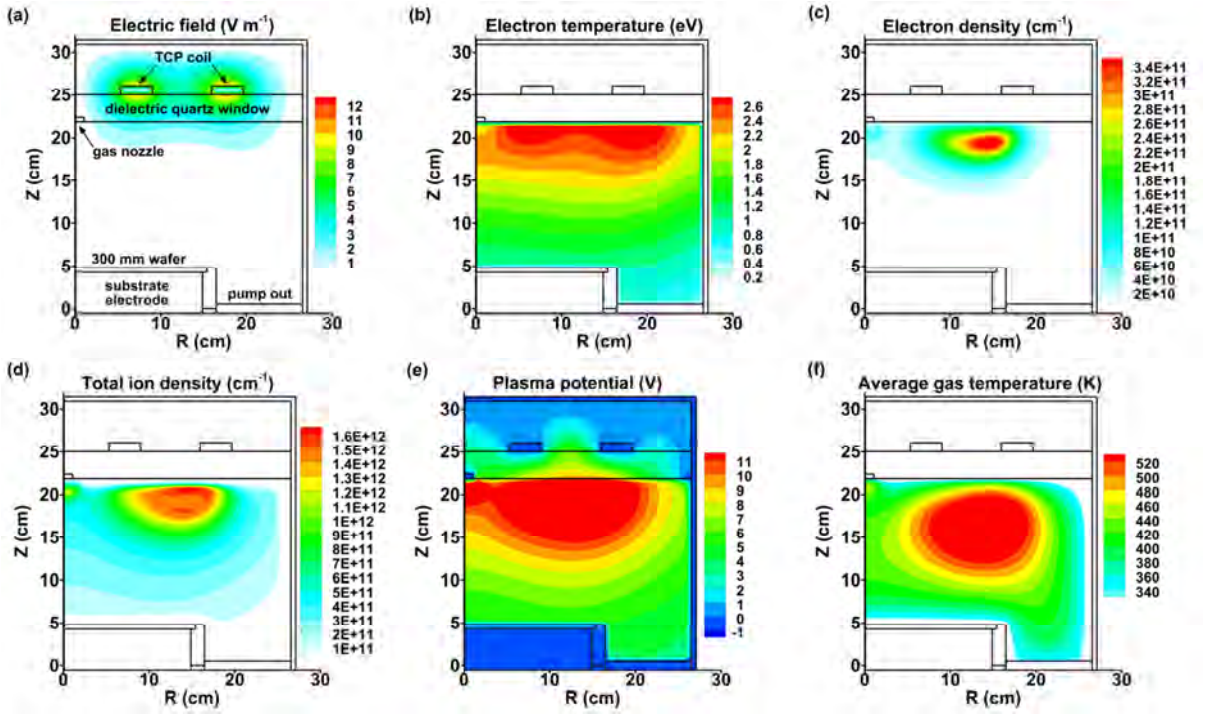

Figure 1. Two-dimensional profiles of the calculated time-averaged source power electric field (a), time-averaged electron temperature (b), electron density (c), total ion density (d), plasma potential (e) and average gas temperature (f). The operating conditions are: 13.56 MHz operating frequency, 40 mTorr chamber pressure, 1000 W source power and 100 sccm total gas flow rate, with a gas mixture of 20% CF_4, 10% CHF_3, 10% H_2, 20% Cl_2, 20% O_2 and 20% HBr.

2. Variation of CF_4 gas fraction

CF_4 is usually the main gas used for Si etching, as it is the source of F atoms, which are the most reactive species for chemical etching. We have varied the gas fraction of CF_4 between 20% and 80%. The volume averaged densities of species that show interesting trends as a function of CF_4 gas fraction are illustrated in **Figure 2a**, together with the total charged species densities and plasma potential in **Figure 2b**. Only the most relevant species and non-obvious trends are shown and discussed.

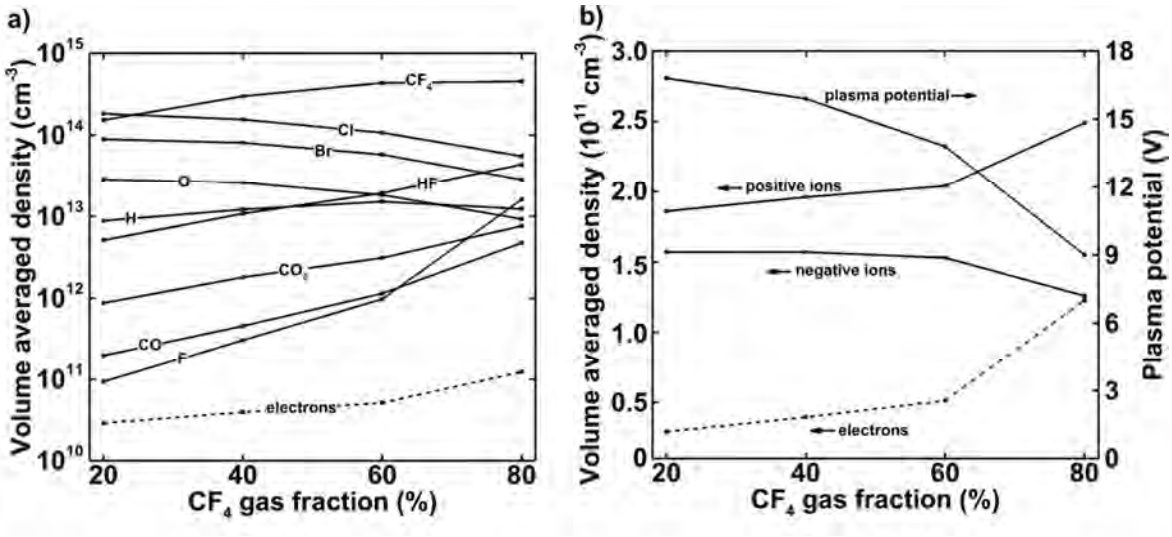

Figure 2. (a) Calculated volume averaged densities of various species as a function of CF_4 gas fraction. Only relevant and unexpected trends are shown. (b) Volume averaged total positive and negative ion and electron densities (left axis) and plasma potential (right axis) as a function of CF_4 gas fraction. The other operating conditions are the same as in **Figure 1**.

As CF_4 is the main source of F atoms in the plasma reactor, the F atom density increases significantly with CF_4 gas fraction, which will usually entail a higher etch rate. However, this will not always be the case, because the F atom density is only in the order of 10^{11}-10^{13} cm^{-3}, and thus much lower than the density of several other plasma species responsible for etching, like the Cl atoms (see **Figure 2a**). For instance, the Cl atom density is more than 3 orders of magnitude higher at 20% CF_4, but it clearly drops upon increasing CF_4 fraction, and at 80% CF_4 it is only about 10 times higher than the F atom density. The fact that it is still higher than the F atom density, even when the F atom source (CF_4 gas) is much more abundant than the source of Cl atoms (i.e. Cl_2 gas) can be explained because Cl_2 is much easier dissociated than CF_4. Indeed, electron impact dissociation of Cl_2 happens easily due to the relatively low bond strength of 2.5 eV and the low threshold for dissociation of 3.12 eV, compared to a threshold of 12.0 eV for CF_4 (and 7.0 eV for CF_3).[31] This suggests that mainly low energy electrons will be responsible for Cl_2 dissociation. The conclusion here is that an increase of CF_4 gas will practically always result in a higher etch rate due to the formation of more highly reactive F atoms. However, when CF_4 would be mixed with Cl_2, it is not unlikely to find a steady or even decreasing etch rate, because the drop in Cl atom density is much more significant compared to the increase in F density. It is generally known that etching with F atoms occurs roughly 9 times faster

than with Cl atoms, but since the density of Cl is a few orders of magnitude higher than the density of F, Cl atoms might contribute more to the etch rate than the F atoms in these situations.[63] On a side note, if Cl_2 would be mixed with SF_6 instead of CF_4, we do expect an increase in the etch rate, as is found experimentally, because SF_6 is a better source for F atoms compared to CF_4 (due to lower threshold for dissociation).[65]

Overall it is found that the CF_x product densities increase as a function of CF_4 gas fraction, along with the F-containing cross-products (like COF_2, COF, FO and HF), while the densities of the other components, like CHF_x, Cl, Br, O etc. (see **Figure 2a**) decrease, as expected. However, there are a few interesting exceptions, as explained here below.

Apparently, more H atoms are present at a higher CF_4 gas fraction, even if the fractions of feed gases CHF_3 and H_2 decrease, which is important to keep in mind for the etching process, as H atoms can significantly alter the Si structure. Obviously, the total amount of hydrogen decreases with rising CF_4 gas fraction, as is logical, but a large fraction of H_2 is lost in a reaction with F to form HF and H (see **Table 3, part 3**). The rate of this reaction depends on the F atom density, which increases with rising CF_4 gas fraction, and this results in a higher H atom density along with that of the F atoms.

The other product of this reaction, which has a significant influence on the etch rate, is HF. HF is a cross-product with a relatively high density (see **Figure 2a**), because it has the strongest chemical bond in the system (5.86 eV) and it is therefore not easily lost through chemical reactions. The formation of HF is therefore an efficient sink for the reactive F atoms, which will entail a lower etch rate, especially when the H_2 fraction is relatively high. It must be noted that HF is also often used to etch Si, but this is usually performed in wet etch chemistries, because HF reacts much slower than F atoms during dry plasma etching.[66]

Other products that become slightly more abundant with increasing CF_4 gas fraction are CO_2 and CO. CO_2 is also a very stable product and a proper sink for reactive O atoms. CO_2 and CO are formed from the ongoing oxidation of the CF_x products to COF or COF_2, and eventually to CO_2 and CO. The densities of CO_2 and CO are therefore correlated to those of the CF_x products, which increase with rising CF_4 gas fraction.

It is interesting to mention, that at 20% CF_4, the most abundant negative ion is Br^- even when F^- and Cl^- are more electronegative. These negative ions are formed through electron impact dissociative attachment and these reactions typically have very low or no threshold and hence they easily happen in the plasma. The Br^- density is about one order of magnitude higher at 20% CF_4 and 20% HBr, due to the fact that the cross section for dissociative attachment from HBr* is considerably larger than the corresponding cross sections for the other reactions. As a result, the dominant process for negative ion formation is that of Br^-. As the fraction of CF_4 becomes higher, F^- becomes the dominant anion, but the decrease of Br^- is more significant, resulting in an overall drop in the negative ion density as shown in **Figure 2b**. This drop in negative ion density is also found when increasing all other gas components (see next sections) except for HBr, which suggests that Br^- is indeed the dominant anion defining the trend in the total anion density.

The dominant Br^- formation and its drop at higher CF_4 gas fraction eventually also affects the electron density and the positive ion density. When less HBr (and HBr*) is present in the reactor, less negative ions are created and thus more free electrons exist that can entail ionizations and create, in turn, positive ions. As a result, the electron and positive ion density increase along with the CF_4 fraction. This is an interesting conclusion, because in more simple gas mixtures (like CF_4/Cl_2), an increase of the CF_4 fraction actually entails a decrease of the electron and positive ion density, as was found experimentally[67] and also checked in our simulations (for the simple case of a CF_4/Cl_2 mixture). It is due to the presence of HBr in the gas mixture, which causes a significant depletion of free electrons into the formation of Br^-, that this trend of increased electron density with increasing CF_4 gas fraction (and thus lower HBr fraction), is observed in the current simulations."

Furthermore, the plasma potential decreases as a function of rising CF_4 fraction as presented in **Figure 2b**. The trends for electron density and plasma potential are in fact often inversely proportional, as the plasma potential is related to the electron temperature, which is typically inversely related to the electron density.[68] Indeed, a lower electron density means that a certain amount of power is deposited to fewer electrons, so these electrons will be accelerated more strongly, increasing the overall electron temperature.

It can be concluded that more CF_4 gas in the mixture will entail a higher etch rate for several reasons. More highly reactive F atoms are introduced, as well as more positive ions important for sputtering. However, it must be noted that these effects will not always result in an overall higher etch rate, depending on the type of mixture. For example, when CF_4 is mixed with Cl_2, increasing the CF_4 fraction (and thus decreasing the Cl_2 fraction) results in a more significant drop in the density of Cl atoms than a rise in the density of F atoms, as was also observed in literature.[10] Thus, if CF_4 and Cl_2 are mixed without O_2, it can therefore occur that the etch rate actually drops when increasing the CF_4 gas fraction, in spite of the fact that the F atoms are more reactive than Cl atoms. Finally, due to the aggressive etch-inhibiting nature of oxygen, when O_2 is present in the CF_4 mixture, increasing the CF_4 gas fraction will always result in a higher etch rate, simply because the partial gas pressure of O_2 becomes lower in the process and other gas components like Cl_2 and HBr become less relevant in influencing the overall etch rate.

3. Variation of H_2 gas fraction

H_2 is often mixed with CF_4 to tune the sidewall composition during Si etching. A CF_xH_y polymer layer is created on the sidewalls and its stability or thickness can be tuned by controlling the ratio between F and H, in addition to adding O_2. A higher H_2 fraction will therefore entail a lower overall etch rate, as H is less reactive towards Si than F, Cl and Br, and it will thus not form so much of the volatile etch product (SiH_4) than its halogen-counterparts. In addition, increasing the H_2 fraction will also result in a higher fraction of H^+, H_2^+ and H_3^+ ions, which generally have a much lower sputter yield than the other positive ions, due to their small mass. Varying the H_2 fraction therefore also allows control of the physical sputter rate during plasma processing. The volume averaged densities of the most relevant species as a function of H_2 fraction are shown in **Figure 3a**, together with the total charged species densities and plasma potential in **Figure 3b**.

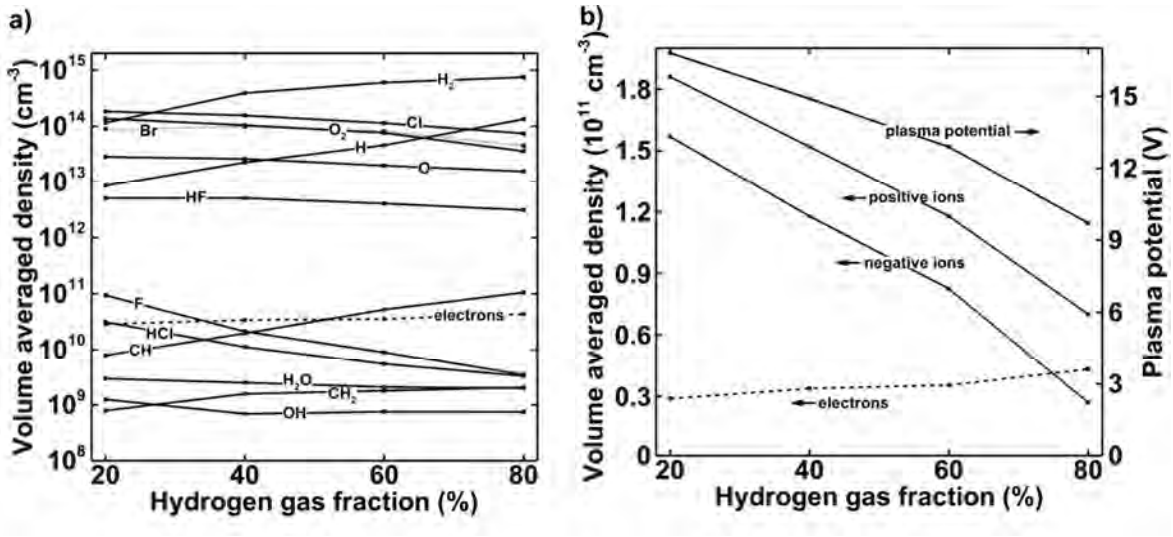

Figure 3. (a) Calculated volume averaged densities of various species as a function of H_2 gas fraction. Only relevant and unexpected trends are shown. (b) Volume averaged total positive and negative ion and electron densities (left axis) and plasma potential (right axis) as a function of H_2 gas fraction. The other operating conditions are the same as in **Figure 1**.

As expected, the H atom density increases as a function of increasing H_2 feed gas fraction, along with some other cross-products like CH and CH_2, while the densities of the other important species for etching (i.e., Cl, F, O and Br) all decrease. H_2O, OH and HCl become less abundant when utilizing more H_2 feed gas, which might be unexpected at first, while HF seems to have an almost constant density within the range of 20-80% H_2. These products all (slightly) decrease in abundance as a function of H_2 gas fraction, simply because their other source terms, like O-, Cl- and F-containing species become less abundant. HF and HCl can both be used to wet-etch Si, but for dry plasma etching, these species are less reactive than the F and Cl atoms.[18] The formation of HF and HCl is therefore an effective sink for these reactive atoms.

The most important losses for electrons, except for the walls, are dissociative attachment reactions, forming F^-, Cl^-, O^- and Br^- ions. These electron impact reactions have low or no threshold energies and are therefore also the most important processes for overall dissociation of the feed gases. For this reason, in most cases, more negative ions are present than free electrons. However, when H_2 becomes more abundant, dissociative attachment becomes less important, and the density of negative ions drops significantly (see **Figure 3b**). At the same time, H_2 has the highest ionization potential (i.e., 15.43 eV) of all gas components, thus it becomes more and more difficult to create ions in general. As

a result, also the total positive ion density drops. In other words, at high H_2 fractions, less electrons and positive ions are created, but also less electrons are lost upon creation of negative ions, which results eventually in a slight increase in electron density within the range of 20-80% H_2. The fact that the density of Br^- drops significantly, as explained in the previous section, also contributes to the increase in free electron density at higher H_2 fractions. As explained in the previous section, the plasma potential and electron density are inversely correlated, so it is expected that the plasma potential drops at higher H_2 fractions.

It can be concluded that the addition of H_2 to the gas mixture will lower the etch rate for many reasons. The most obvious one is that the densities of the etching gases (i.e., CF_4, HBr and Cl_2) and the passivating gases (i.e., O_2), as well as the positive ion densities, all decrease, which results in more moderate etching, but also less pronounced passivation layer formation due to oxygen, as well as less sputtering. Especially sputtering will be reduced, not only due to the lower overall positive ion density at higher H_2 fractions, but also because more H^+, H_2^+ and H_3^+ are formed, which have very low sputter yields due to their small masses. H_2 is therefore an interesting gas if more moderate overall etching is needed, like in the case where ultra-thin layers or ultra-small features must be etched, as found in the current technology node.[68]

4. Variation of Cl_2 gas fraction

Cl_2 is very useful for the selective etching of Si, while keeping Si_3N_4 or SiO_2 layers intact. Si_3N_4 and SiO_2 materials are typically used as masks during selective plasma etching of Si with halogen-based plasmas.[18] This is in contrast to F atoms, which are more aggressive chemical etchers and will also etch SiO_2, but at a significantly lower rate than Si. If a high selectivity is required, it might thus be more useful to use Cl_2 instead of fluorine-based gases, or to create a proper mixture of both.

The volume averaged densities of the most relevant species as a function of Cl_2 gas fraction between 20% and 80% are shown in **Figure 4a**, together with the total charged species densities and plasma potential in **Figure 4b**.

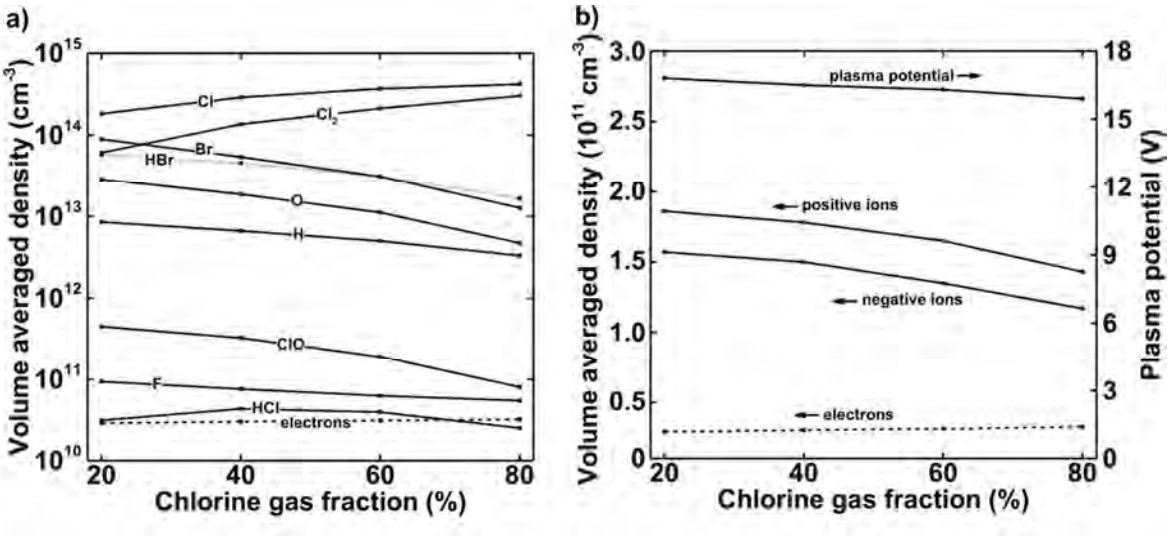

Figure 4. (a) Calculated volume averaged densities of various species as a function of Cl_2 gas fraction. Only relevant and unexpected trends are shown. (b) Volume averaged total positive and negative ion and electron densities (left axis) and plasma potential (right axis) as a function of Cl_2 gas fraction. The other operating conditions are the same as in **Figure 1**.

As mentioned earlier, Cl_2 has a relatively weak bond (i.e., 2.5 eV), which explains why it is highly dissociated in the plasma and why the density of atomic Cl always exceeds that of Cl_2, even if the dissociation degree decreases at higher Cl_2 gas fraction. The density of atomic Cl is indeed always significantly higher than that of Cl_2 for all gas compositions considered in this study. Cl_2 is quickly consumed due to the relatively easy electron impact dissociation, but also due to heavy particle reactions with O* to form ClO. The density of O* is relatively high compared to the electron density, so the reaction of Cl_2 with O* to form ClO is also an important loss process for Cl_2. As the fraction of Cl_2 feed gas becomes larger, the overall O_2 fraction drops, and thus also the O* density, resulting in a reduction of the dissociation degree of Cl_2, as well as the density of ClO (see **Figure 4a**).

Again, as expected, at higher Cl_2 contents, the densities of the most reactive species F, Br, O and H are lower. The only exception is the wet-etch cross-product HCl, which finds a maximum abundance around 40% Cl_2, when both chlorine and hydrogen are sufficiently present.

Furthermore, the total amount of bromine in the plasma per definition decreases with increasing fraction of Cl_2, but HBr actually becomes relatively more abundant than Br, at high Cl_2 content. HBr (like HBr*) is lost by electron impact dissociation or ionization, and by the reaction with H to form Br and H_2. The H atom density decreases much more significantly with rising Cl_2 gas

fraction (due to the accumulated decrease of CHF_3, H_2 and HBr feed gas) than the electron density which increases only slightly (see **Figure 4**). As a result, the formation of Br by HBr dissociation is reduced at high Cl_2 gas fractions, resulting in less Br atoms than expected at higher Cl_2 fractions, which is important to keep in mind for finding a balanced selective etching process if Cl_2 and HBr are mixed.

Cl_2 also has a lower threshold for direct electron impact ionization (11.47 eV) than the other gas components. This explains why the electron density increases (albeit only slightly) with Cl_2 gas fraction (see **Figure 4b**). As mentioned earlier, a higher electron density results in a lower average electron temperature and hence a lower plasma potential, as also illustrated in **Figure 4b**.

Similarly to its low threshold for dissociation, Cl_2 also has a relatively low threshold for ionization compared to the other gas components used, as mentioned earlier. As a result, one would expect more ions at higher Cl_2 content, but the opposite seems to be true, as the electron density only increases slightly and the total ion densities decreases as a function of Cl_2 gas fraction (see **Figure 4b**). One must keep in mind that, due to the low dissociation threshold, actually more atomic Cl is present than Cl_2 gas, and atomic Cl has a slightly higher threshold for ionization compared to the other gases. In the end, the drop in total positive ion density is thus logical. As mentioned in section 2, the negative ion density drops mainly due to the lower fraction of HBr (to create Br^-).

It can be concluded that a higher Cl_2 feed gas fraction will result in a higher chemical etch rate due to the presence of more Cl atoms, but also in less physical sputtering due to a smaller abundance of positive ions. Cl_2 is therefore a perfect gas component to tune the ratio between isotropic chemical etching and anisotropic ion sputtering for etch profile control.

5. Variation of O_2 gas fraction

O_2 is often added to a halogen-based gas to tune the ratio between etching and oxidation of silicon. When Si is converted to SiO_2, it can no longer be chemically etched by Cl and Br, thus drastically reducing the chemical etch rate. SiO_2 can still be etched with F, but it proceeds significantly slower than for pure Si. O_2 is therefore most suitable for sidewall control of the trench profile and the etch

rate is often very sensitive to the amount of oxygen in the gas mixture.[64] The volume averaged densities of the most relevant species as a function of O_2 gas fraction are shown in **Figure 5a**, together with the total charged species densities and plasma potential in **Figure 5b**.

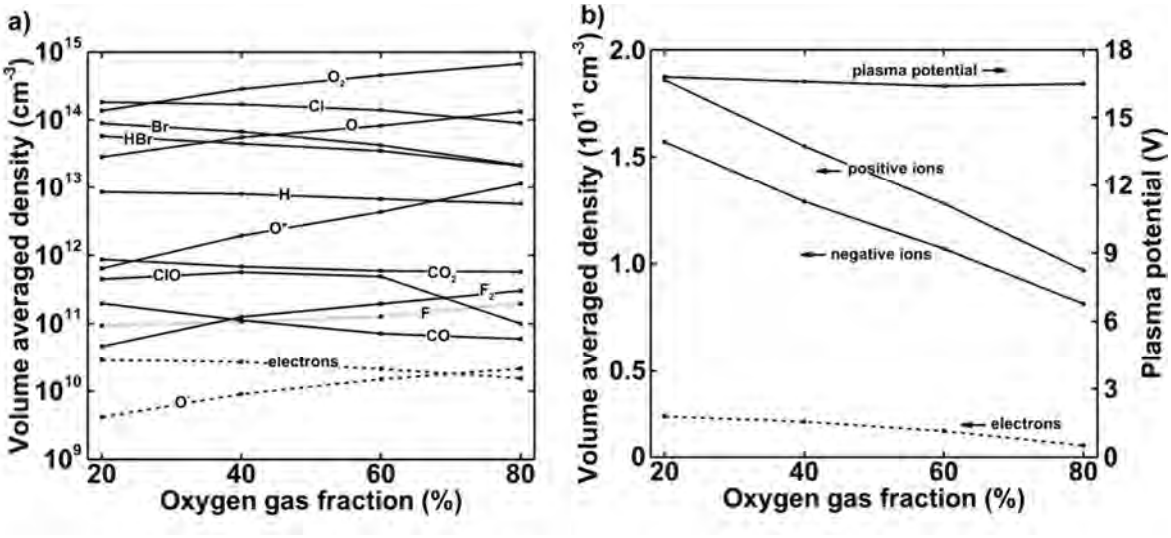

Figure 5. (a) Calculated volume averaged densities of various species as a function of O_2 gas fraction. Only relevant and unexpected trends are shown. (b) Volume averaged total positive and negative ion and electron densities (left axis) and plasma potential (right axis) as a function of O_2 gas fraction. The other operating conditions are the same as in **Figure 1**.

The dissociation degree of O_2 is much lower compared to that of Cl_2 due to the stronger double O=O bond (i.e., 5.2 eV vs. 2.5 eV). As a result, molecular oxygen is more abundant than atomic oxygen, as opposed to Cl and Cl_2 under comparable conditions (see **Figure 4a and 5a**). Also the ionization threshold for O_2 (i.e., 12.06 eV) is slightly higher than for most other gas components. Thus, the more O_2 present in the plasma, the lower the electron density, as is clear from **Figures 5a** and **5b**. As explained in section 2, this will result in a higher average electron temperature and plasma potential, and thus in a slightly higher positive ion energy when bombarding the wafer, although the change in plasma potential is only minimal within the range of 20-80% O_2. On the other hand, the positive ion flux clearly drops upon increasing O_2 fraction, so that the sputter rate, which is linearly correlated to the positive ion flux, will drop. The plasma density in general also decreases with rising O_2 fraction, which results in a lower dissociation degree of all gas components (because of lower electron impact dissociation), as illustrated in **Figure 5a** for the HBr and Br densities.

It is interesting to note that the densities of F and F_2 actually increase as a function of O_2 feed gas fraction. This is important because the competition between fluorination and oxidation of the silicon strongly affects the overall etch rate and trench profile control. Increasing the O_2 fraction in the plasma will thus reduce or inhibit the chemical etch rate due to the formation of a SiO_2-based passivation layer, as is found experimentally as well[12], but not because there would be less F atoms present. The reason that the F atom density does not drop significantly, in spite of the lower CF_4 and CHF_3 gas fractions, is because O and O* react with CF_x products to form COF_x + F (see **Table 3, part 3**) and these reactions are an important source for the F atoms. The densities of CF_x species obviously drop upon increasing O_2 fraction, but the densities of O and O* increase at the same time (see **Figure 5a**), resulting in an overall higher production of the F atoms (and consequently also of F_2) when increasing the O_2 gas fraction.

Most other reactive species (apart from F) follow predictable trends, i.e., Cl, H and Br become less abundant when the O_2 feed gas fraction is increased. ClO, on the other hand, shows a maximum in the range of 40-60% O_2, similar to the case where Cl_2 was varied (see **Figure 4a**).

With respect to the etch rate, increasing the O_2 fraction in the plasma will always lower the etch rate due to more oxidation of the wafer surface, which results in an enhanced passivation layer formation, thus strongly limiting chemical etching. In addition, the etch rate is further reduced due to a lower plasma density and lower positive ion flux towards the wafer at higher O_2 content, and therefore less sputtering occurs. However, the density of the most aggressive chemical etchers, i.e., the F atoms, does actually increase with rising O_2 gas fraction, as explained above. This is relevant to note because the exact balance between fluorination and oxidation is important for fine-tuning the overall etch rate and for control of the sidewall profile.

6. Variation of HBr gas fraction

As mentioned in the introduction, HBr can be added to fine-tune the etch process and is especially useful when a high control of the preferentially low etch rate is necessary. Br is significantly less reactive towards Si than Cl and F, making it suitable to moderately etch very thin layers. The volume

averaged densities of the most relevant species as a function of HBr gas fraction are presented in **Figure 6a,** while the total charged species densities and plasma potential are shown in **Figure 6b**.

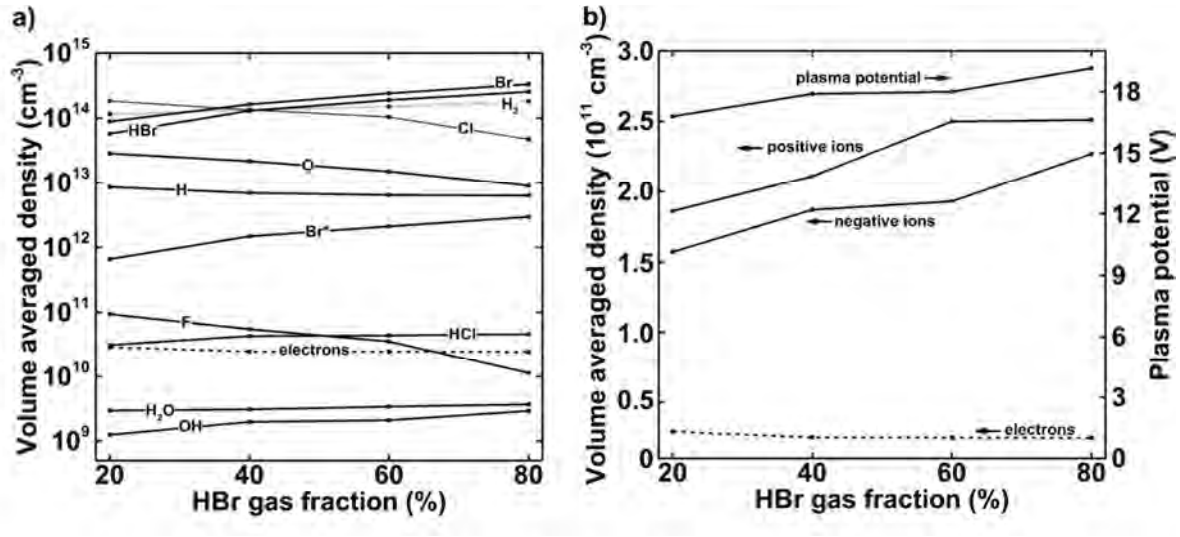

Figure 6. (a) Calculated volume averaged densities of various species as a function of HBr gas fraction. Only relevant and unexpected trends are shown. (b) Volume averaged total positive and negative ion and electron densities (left axis) and plasma potential (right axis) as a function of HBr gas fraction. The other operating conditions are the same as in **Figure 1**.

The evolution of the densities of most species as a function of HBr gas fraction is like expected. When HBr becomes more abundant in the plasma, the densities of Br and Br* increase and most other chemical components (e.g., Cl, O and F) decrease, with some exceptions as explained here below.

A higher HBr gas fraction entails lower CHF_3 and H_2 partial gas pressures, which results in a perhaps unexpected overall slight decrease of the H atom density in the plasma, as is clear from **Figure 5a**.

Furthermore, some other products, i.e., H_2O, OH and HCl, become more abundant with rising HBr gas fraction, which might also be unexpected at first. H_2O, OH and HCl are efficient sinks for O and Cl atoms, respectively, because OH and HCl are only significantly reactive in wet chemistries. These products are practically always lost through electron impact ionization or dissociation (see **Table 2**) and since the electron density decreases with rising HBr gas fraction, so does the loss rate for these products, even when the presence of oxygen becomes low. Furthermore, another loss process for these species is the reaction with H. As the H atom density also decreases more abruptly than the densities of the sources for OH (see **Figure 6a**), this also results in an overall higher net production rate and thus a higher density for OH and H_2O as a function of HBr feed gas fraction.Similar to O_2

(see section 5), HBr has a relatively high ionization threshold (12.74 eV), so one would expect a drop in electron density with increasing HBr gas fraction. This is indeed clear from **Figure 6a and 6b**, although the drop is only moderate. However, for HBr the situation is slightly more complex. HBr*, which has a density about one order of magnitude lower than HBr, can be ionized much more easily than ground state HBr and the process of electron impact ionization has in fact the lowest threshold of all molecules included in the model (i.e., 4.3 eV; See **Table 2**) for the formation of positive ions and free electrons. As a result, the positive ion density increases strongly with HBr fraction. The free electron density would follow a similar trend, but another process is also very important. Indeed, a large fraction of HBr* is lost into preferential formation of Br^- through dissociative attachment. As an end result, the electron density seems to slightly decrease as a function of HBr fraction, while the total positive and negative ion densities significantly increase, as presented in **Figure 6b**.

Thus, introducing more HBr in the plasma results in reduced chemical etching due to a drop in the densities of Cl and F that are more reactive than Br atoms. However, the ion sputter rate will significantly increase due to the higher densities of HBr^+ and Br^+ in the plasma at higher HBr feed gas fraction, if a bias would be applied. Even though HBr is often used together with H_2 or O_2 to etch Si, when mixed with F- and Cl-containing gases[18], HBr creates the same diluting effects as Ar or He, where an increased fraction results in less chemical etching but more (physical) sputtering. This is important for finding a proper balance between chemical etching and physical sputtering and eventually successful anisotropic etching.

IV. Conclusions

We have computationally investigated high-density low-pressure $CF_4/CHF_3/H_2/Cl_2/O_2$/HBr plasmas to better understand the bulk plasma chemistry of this complex mixture during wafer processing.

Each chemical component of the feed gas mixture is varied between 20% and 80% and the evolution of all plasma species densities is tracked to obtain more insight in the total bulk plasma chemistry of these complex mixtures and how this might affect the etch rate.

It is observed that a higher CF_4 gas fraction results in a higher etch rate, not due to an increased density of reactive F atoms, but mainly due to a lower content of oxygen which inhibits chemical etching. Under the investigated conditions, increasing the CF_4 fraction produces more F atoms for chemical etching as expected, but it also more prominently lowers the density of Cl atoms. The latter are less reactive than the F atoms, but they have much higher densities, making them the most important etchers. In the case when only CF_4 and Cl_2 would be mixed without oxygen, it can therefore occur that the etch rate actually drops when increasing the CF_4 gas fraction. Furthermore, the electron density typically drops upon increasing CF_4, for example when mixed with Cl_2. However, depending on the kind of the other gas components, CF_4 gas can sometimes also enhance the free electron density. This is the case when mixed with HBr for example.

The addition of H_2 to the etching mixture will lower the etch rate for various reasons. The densities of the etching gases (i.e., CF_4, HBr and Cl_2) and the passivating gas (i.e., O_2) as well as the positive ion densities all decrease due to an overall lower plasma density, which results in less etching, less passivation layer formation and less sputtering. Especially sputtering will be reduced, not only due to the lower overall positive ion density at higher H_2 fractions, but also because more H^+, H_2^+ and H_3^+ are formed which have very low sputter yields. H_2 therefore acts as a diluting agent, making it suitable for etching thin or small features with high control.

In contrast, a larger Cl_2 fraction will result in a higher chemical etch rate due to the higher presence of Cl atoms, but also in less physical sputtering due to a smaller abundance of positive ions. In the investigated conditions Cl atoms are always the most import species for the etching process, even when F atoms are more reactive, due to their flux being a few orders of magnitude higher than that of the F atoms. Cl_2 is therefore a perfect gas component to tune the ratio between isotropic chemical etching and anisotropic ion sputtering for etch profile control.

With respect to the etch rate, increasing the O_2 fraction in the plasma will always lower the etch rate due to more oxidation of the wafer surface, which results in an enhanced passivation layer formation, thus strongly limiting chemical etching. In addition, the etch rate is further reduced due to a lower plasma density and lower positive ion flux towards the wafer at higher O_2 content, and therefore less sputtering occurs. However, the density of the most aggressive chemical etchers, i.e.,

the F atoms, does actually increase with rising O_2 gas fraction as explained above. This is relevant to note because the exact balance between fluorination and oxidation is important for fine-tuning the overall etch rate and for control of the sidewall profile.

Finally, introducing more HBr in the plasma will result in reduced chemical etching due to a smaller amount of Cl and F atoms, which are more reactive than Br. In contrast, the ion sputter rate will significantly increase with rising HBr fraction due to the higher densities of HBr^+ and Br^+ in the plasma. Even though HBr is often used together with H_2 or O_2 to etch Si, when mixed with F- or Cl-containing gases[18], it creates the same diluting effects as Ar or He, where an increased fraction results in less chemical etching but more (physical) sputtering, which is important for finding a proper balance between chemical etching and physical sputtering and eventually successful etching profile control.

Acknowledgements

We acknowledge the Fund for Scientific Research Flanders (FWO) for financial support of this work. This work was carried out in part using the Turing HPC infrastructure at the CalcUA core facility of the Universiteit Antwerpen, a division of the Flemish Supercomputer Center VSC, funded by the Hercules Foundation, the Flemish Government (department EWI) and the University of Antwerp.

References

[1] Moore G, *Electronics* **38** 8 1965
[2] Mogab C, Adams A and Flamm D, *J. Appl. Phys*. **49** 3796 1978
[3] D'Agostino R, Cramarossa F, De Benedistis S and Ferraro G, *J. Appl. Phys.* **52**, 1259 1981
[4] Donnelly V, Flamm D, Dautremont-Smith W and Werder D, *J. Appl. Phys.* **55** 242 1984
[5] Plumb I and Ryan K, *Plasma Chem. Plasma Process.* **6** 205 1986
[6] Dalvie M and Jensen K, *J. Vac. Sci. Technol. A* **8** 1648 1990
[7] Knizikevicius R, Galdikas A and Grigonis A, Vacuum **66** 39 2002
[8] Kim J, Kim Y and Lee W, *J. Appl. Phys.* **78** 2045 1995
[9] Kimura T and Noto M, *J. Appl. Phys.* **100** 063303 2006
[10] Rangelow I, *J. Vac. Sci. Technol. A* **21** 1550 2003
[11] Jansen H, Gardeniers H, De Boer M, Elwenspoek M and Fluitman J, *J. Micromech. Microeng.* **6** 14 1996
[12] Dussart R, Tillocher T, Lefaucheux P and Boufnichel M, *J. Phys. D: Appl. Phys*. **47** 123001 2014

[13] Oehrlein G and Williams H, *J. Appl. Phys.* **62** 662 1987

[14] Tinck S, Boullart W and Bogaerts A, *J. Phys. D: Appl. Phys*. **42** 095204 2009

[15] Zhang Y, Tinck S, De Schepper P, Wang N and Bogaerts A, *J. Vac. Sci. Technol. A* **33**(2) 021310 2015

[16] D'Agostino R and Flamm D, *J. Appl. Phys*. **52** 162 1981

[17] Gul B, Tinck S, De Schepper P, Rehman A and Bogaerts A, *J. Phys. D: Appl. Phys.* **48** 025202 2015

[18] Wasa K, Kitabatake M and Adachi H, *Thin film materials technology: sputtering of control compound materials*, Springer Science & Business Media 2004

[19] Meichsner J, Schmidt M, Schneider R and Wagner H, *Nonthermal plasma chemistry and physics*, CRC Press 2012

[20] Guinn K, Cheng and Donnelly V*, J. Vac. Sci. Technol. B* **13** 214 1995

[21] Efremov A, Kim Y, Lee H and Kwon K*, Plasma Chem. & Plasma Proc*. **31** 259 2011

[22] Cunge G, Inglebert R, Joubert O, Vallier L and Sadeghi N, *J. Vac. Sci. Technol. B* **20** 2137 2002

[23] Kushner M, *J. Phys. D: Appl. Phys.* **42** 194013 2009

[24] Knizikevičius R, *Vaccuum* **82** 1191 2008

[25] Ho P, Johannes J, Buss R and Meeks E, *J. Vac. Sci. Technol. A* **19** 2344 2001

[26] Hassouni K, Leroy O, Farhat S, Gicquel A, *Plasma Chem. and Plasma Proc*. **18** 325 1998

[27] Lee C and Lieberman M, *J. Vac. Sci. Technol. A* **13** 368 1995

[28] Tinck S and A Bogaerts A, *Plasma Sources Sci. Technol.* **20** 015008 2011

[29] Hwang H, Meyyappan M, Mathad G and Ranade R, *J. Vac. Sci. Technol. B* **20** 2199 2002

[30] De Bleecker K, Bogaerts A, Goedheer W and Gijbels R*, Phys. Rev. E* **69** 056409 2004

[31] Bonham R, *Jpn. J. Appl. Phys.* **33** 4157 1994

[32] Meeks E, *J. Electrochem. Soc*. **144** 357 1998

[33] Tarnovsky V and Becker K, *J. Chem. Phys*. 98 7869 1993

[34] Hayashi M and Nimura T, *J. Appl. Phys*. **54** 4879 1983

[35] Zhang D and Kushner M, *J. Vac. Sci. Technol. A* **18** 2661 2000

[36] Vriens L, *Phys. Lett.* **8** 260 1964

[37] Kushner M and Zhang D, *J. Appl. Phys.* 88 3231 2000

[38] Yang Y and Kushner M, *Plasma Sources Sci. Technol.* **19** 055011 2010

[39] Corrigan S, *J. Chem. Phys.* **43** 4381 1965

[40] Hayashi M, *J. Phys.* **40** 45 1979

[41] Chan C, "Reaction cross-sections and rate coefficients related to the production of positive ions", Lawrence Berkeley Lab. Report No. LBID-632 1983

[42] Banks P, *Planet. Sp. Sci.* **14** 1085 1966

[43] Rauf S and Kushner M, *J. Appl. Phys.* **82** 2805 1997

[44] Tachibana K *Phys. Rev. A* **34** 1007–15 1986

[45] Horacek J and Domcke W, *Phys. Rev. A* **53** 2262 1996

[46] Lowke J, Phelps A and Irwin C, *J. Appl. Phys*. **44** 4664 1973

[47] Atkinson R, Baulch D, Cox R, Crowley J, Hampson R, Hynes R, Jenkin M, Rossi M and Troe J, *Atmos. Chem. Phys.* **4** 1461 2004

[48] Hayashi M, *"Electron Collision Cross Sections For Molecules Determined From Beam And Swarm Data In Swarm Studies And Inelastic Electron-Molecule Collisions",* Spinger-Verlag New York 1987

[49] Thorsteinsson E and Gudmundsson J, *Plasma Sources Sci. Technol.* **19** 055008 2010

[50] Shuman N, Wiens J, Miller T and Viggiano A*, J. Chem. Phys*. **140** 224309 2014

[51] Zhao S, Gao F, Wang Y and Bogaerts A, *Plasma Sources Sci. Technol.* **21** 025008 2012

[52] Song S and Kushner M, *Plasma Sources Sci. Technol*. **21** 055028

[53] Woodall J, Agundez M, Markwick-Kemper A and Millar T, *Astron. Astrophys.* **466** 1197 2006

[54] A. Bogaerts A and Gijbels R, *Spectrochim. Acta B* **57** 1071 2002

[55] Kushner M, *J. Appl. Phys.* **63** 2532 1988

[56] Ikezoe Y, Matsuoka S, Takabe M and Viggiano A "*Gas Phase Ion–Molecule Reaction Rate Constants"* 1986 (Tokyo: Mass Spectroscopy Society of Japan)

[57] Burgess D, Zacharaiah M, Tsang W and Westmoreland P, *Prog. Energy Combust. Sci.* **21** 453 1995

[58] Voloshin D, Klopofskiy K, Mankelevich Y, Popov N, Rakhimova T and Rakhimov A, *IEEE Trans. Plasma Sci.* **35** 1691 2007

[59] Harding L, Guadagnini R and Schatz G, *J. Phys. Chem*. **97** 5472 1993

[60] Tsai C and McFadden D*, J. Phys. Chem.* **93** 2471 1989

[61] M. J. Kushner, J. Appl. Phys. 1993, 74, 6538

[62] Ham Y, Efremov A, Yun S, Kim J, Min N and Kwon K, *Thin Solid Films* **517** 4242 2009

[63] Tian W, Weigold J and Pang S, *J. Vac. Sci. Technol. B* **18** 1890 2000

[64] Tinck S, Shamiryan D and Bogaerts A, *Plasma Process. Polym*. **8** 490 2011

[65] Kang S, Lee S, Lee H, Kwon K,Choi B, Song Y, Lee J and Choa K, *J. El. Soc*. **146** 4626 1999

[66] Takahagi T, Nagai I, Ishitani A, Kuroda H and Nagasawa *, J. Appl. Phys*. **64**(7) 3516 1988

[67] Boyd T and Sanderson J, "*The Physics of Plasmas"*, 1st ed. Cambridge University Press 2003

[68] Efremov A, Kim D and Kim C*, J. Kor. Phys. Soc*. **43** 1042 2003

[69] *International Technology Roadmap for Semiconductors*, www.itrs.net